THESIS ON NATURAL AND EXACT SCIENCES B144

Deposition of In_2S_3 Thin Films by Chemical Spray Pyrolysis

KAIRI OTTO

TUT PRESS

TALLINN UNIVERSITY OF TECHNOLOGY
Faculty of Chemical and Materials Technology
Department of Materials Science
Laboratory of Thin Film Chemical Technologies

Dissertation was accepted for the defence of the degree of Doctor of Philosophy in Chemistry and Materials Technology on October 1, 2012

Supervisor: Dr. Malle Krunks, Leading Research Scientist,
Department of Materials Science, Tallinn University of Technology

Opponents: Dr. Kaupo Kukli, Lead Research Fellow in Material Science,
Institute of Physics, Faculty of Science and Technology,
University of Tartu, Estonia

Dr. Imre Miklós Szilágyi, Research Fellow, Research Group of
Technical Analytical Chemistry of the Hungarian Academy of Sciences,
Department of Inorganic and Analytical Chemistry,
University of Technology and Economics, Hungary

Defence of the thesis: November 27, 2012, at 14:00
Lecture hall: VI-201
Tallinn University of Technology, Ehitajate tee 5, Tallinn

Declaration:

Hereby I declare that this doctoral thesis, my original investigation and achievement, submitted for the doctoral degree at Tallinn University of Technology has not been submitted for any academic degree.

This work has been partially supported by graduate school „Functional materials and technologies" receiving funding from the European Social Fund under project 1.2.0401.09-0079 in Estonia.

ISSN 1406-4723
ISBN 978-9949-23-381-6 (publication)
ISBN 978-9949-23-382-3 (PDF)

LOODUS- JA TÄPPISTEADUSED B144

In_2S_3 õhukesed kiled keemilise pihustuspürolüüsi meetodil

KAIRI OTTO

TTÜ
KIRJASTUS

Table of contents

LIST OF PUBLICATIONS

List of publications

Article I:
K. Otto, A. Katerski, A. Mere, O. Volobujeva, M. Krunks. Spray Pyrolysis Deposition of Indium Sulfide Thin Films. Thin Solid Films, 2011, 519 (10), p. 3055–3060.

Article II:
K. Otto, A. Katerski, O. Volobujeva, A. Mere, M. Krunks. Indium sulfide thin films deposited by chemical spray of aqueous and alcoholic solutions. Energy Procedia, 2011, 3, p. 63–69.

Article III:
K. Otto, I. Oja Acik, K. Tõnsuaadu, A. Mere, M. Krunks. Thermoanalytical study of precursors for In_2S_3 thin films deposited by spray pyrolysis. Journal of Thermal Analysis and Calorimetry, 2011, 105 (2), p. 615–623.

Article IV:
K. Otto, P. Bombicz, J. Madarász, I. Oja Acik, M. Krunks, G. Pokol. Structure and evolved gas analysis (TG/DTA-MS and TG-FTIR) of mer-triclorotris(thiourea)-indium(III), a precursor for indium sulfide thin films. Journal of Thermal Analysis and Calorimetry, 2011, 105 (1), p. 83–91.

Copies of these articles are included in APPENDIX A.

THE AUTHOR'S CONTRIBUTION TO THE PUBLICATIONS

The contribution by the author to the papers included in the thesis is as follows:

Article I:
Deposition of In_2S_3 thin films by chemical spray pyrolysis (CSP), films characterization (XRD, UV-VIS spectroscopy), analysis of the results, notable role in writing.

Article II:
Deposition of In_2S_3 thin films by CSP, films characterization (XRD, UV-VIS spectroscopy), analysis of the results, major role in writing.

Article III:
Synthesization and characterization by FTIR of the precursors for thermal analysis, participation in conduction of thermal analysis of dried precursors (TG/DTA/EGA-FTIR measurements), characterization of solid intermediates and final products by FTIR, analysis of the results, major role in writing.

Article IV:
Participation in conduction of thermal analysis of dried precursors (TG/DTA/EGA-FTIR and TG/DTA/EGA-MS measurements), analysis of the results, major part in writing.

LIST OF ABBREVIATIONS

ALD	Atomic Layer Deposition
BE	Binding Energy
CBD	Chemical Bath Deposition
CSP	Chemical Spray Pyrolysis
CVD	Chemical Vapour Deposition
DSC	differential scanning calorimetry
DTA	Differential Thermal Analysis
DTG	Differential Thermogravimetry
EDX	Energy Dispersive X-ray Spectroscopy
E_g	Optical bandgap
EGA	Evolved Gas Analysis
ETA	Extremely thin absorber
FTIR	Fourier Transform Infrared Spectroscopy
FWHM	Full Width at Half Maximum
JCPDS	Joint Committee on Powder Diffraction Standards
Me-O	Oxygen bonded to a metal
mer	Meridional (ligands and the metal cation are in one plane)
MS	Mass spectroscopy
NIST	National Institute of Standards and Technology
ORTEP	Oak Ridge Thermal Ellipsoid Plot Program
PVD	Physical Vapour Deposition
SC	Solar Cell
SEM	Scanning Electron Microscopy
SILAR	Successive Ionic Layer Adsorption and Reaction
Spray-ILGAR	Spray Ion Layer Gas Reaction
TA	Thermal Analysis
TG	Thermogravimetry
T_s	Substrate temperature
tu	Thiourea
USP	Ultrasonic Spray Pyrolysis
UV-VIS	Ultraviolet-Visible (Spectroscopy)
XPS	X-ray Photoelectron Spectroscopy
XRD	X-Ray diffraction

INTRODUCTION

Indium sulfide (In_2S_3) thin films have been mainly used as a buffer layer in chalcopyrite absorber based solar cells [1 – 4]. Recently, In_2S_3 has been proposed as a host material for an absorber in intermediate band solar cells [5, 6].

In the past decades the application of In_2S_3 thin films in photovoltaic devices has been studied by many research groups [1 – 4]. In_2S_3 thin films can be obtained by different physical and chemical methods; however crystalline, electrical and optical properties of the obtained films depend on the deposition method applied [1]. The chemical spray pyrolysis (CSP) is an economical method, which uses low-cost set-up to produce large-area thin films, and it can be performed in air using short processing times. Researchers at Tallinn University of Technology (TUT), Estonia, have used the CSP method to deposit different thin films for many years. The first studies on the CSP deposition of CdS thin films were conducted by Dr. K. Kerm [7]. Since then the pneumatic CSP equipment has been significantly improved and the ongoing depositions of different metal sulfide (ZnS, $CuInS_2$, CdS, In_2S_3) and metal oxide (TiO_2, ZnO) films have been performed by the research group led by Dr. M. Krunks [8 – 13]. In the Laboratory of Thin Film Chemical Technologies, a nanostructured solar cell, including In_2S_3 as a buffer layer, has been made by CSP using a pneumatic spray set-up [3]. In order to prepare an effective solar cell, it is important to be aware of the properties of each layer in the solar cell structure.

Prior to the present study, only limited number of studies had been made on the deposition of In_2S_3 films by the pneumatic CSP. According to the literature, no studies on the formation of In_2S_3 during the CSP process by using $InCl_3$ and $SC(NH_2)_2$ as starting chemicals have been reported.

This thesis contains a comprehensive study on the effect of the molar ratio of the starting chemicals ($InCl_3$ to $SC(NH_2)_2$) in aqueous or alcoholic spray solutions and various deposition temperatures on the properties of sprayed In_2S_3 films. The formation chemistry of In_2S_3 in the CSP process is studied. Knowledge of formation chemistry is needed to understand and thereby control properties of sprayed In_2S_3 thin films.

Chapter 1 contains the literature review. Chapter 2 describes the preparation of In_2S_3 films by CSP and applied characterization methods, followed by the synthesis of the precursors for the process chemistry study with the characterization and applied thermoanalytical methods. Chapter 3 presents the obtained results along with discussion reported in two main parts. The first part deals with the characterization of the structure and phase composition, the morphology, optical properties and elemental composition of sprayed In_2S_3 films depending on growth temperatures and the molar ratio of starting chemicals ($InCl_3$ to $SC(NH_2)_2$) in aqueous or alcoholic spray solutions. These results are published in papers I and II. The second part of Chapter 3 presents the interaction of starting chemicals in the spray solution, the formation and structure of intermediate complex compound as a precursor for In_2S_3. Thereupon the results of thermal degradation of the precursors

and the formation of In_2S_3 are presented by simultaneous thermogravimetric and differential thermal analysis coupled online with evolved gas analyses by FTIR and MS. The detailed results and discussion of the formation chemistry of In_2S_3 in CSP are published in papers III and IV. Finally, Chapter 4 summarizes the main results of the present study.

This work is financially supported by the Estonian Ministry of Education and Research (Target Financing Project SF0140092s08); the Estonian Science Foundation (grants ETF6954, ETF7788 and ETF9081); Centre of Excellence "Mesosystems - Theory and Applications" (TK114). This work has been partially supported by the projects AR10128 ("New materials for solar energetics"), AR12118 ("Efficient plasmonic absorbers for solar cells") and the Graduate School "Functional materials and technologies" financed by the European Social Fund under the project 1.2.0401.09-0079 in Estonia. Additionally, the Internationalization Programme DoRa Activity 8 is appreciated for support.

1 LITERATURE REVIEW

1.1 General properties of indium sulfide as a material

There are three main phases, InS, In_6S_7 and In_2S_3, existing with different modifications in the In-S system [14 – 17]. The existence of other indium sulfide phases, such as In_3S_4, In_3S_5, In_4S_5 in the In-S system is questionable [14, 16].

The phases of InS, In_6S_7 and In_2S_3 exist in the In-S system under the following conditions:

1. InS – contains indium in the range of 50 – 51 at% and occurs as α- and β-InS. The orthorhombic α-InS transforms into β-InS at temperatures above 657 °C (Fig. 1.1 b).
2. In_6S_7 – contains ~46 at% of indium and exists up to 780 °C (Fig. 1.1 a, b).
3. In_2S_3 – contains indium in the range of 40 – 42 at% (Fig. 1.1 b). In_2S_3 appears in tetragonal, cubic and trigonal crystallographic forms, which are generally named as β-, α- and γ-In_2S_3, respectively [18].
   - The tetragonal β-In_2S_3 with the space group of $I4_1/amd$ is the most stable phase at room temperature and exists up to 414 °C (Fig. 1.1). In the tetragonal In_2S_3 structure, the cation vacancies are ordered along a 4_1 screw, the unit cell consists of three spinel cubes stacked parallel to the c-axis (Fig. 1.2) with the lattice parameters a=b=7.617 Å and c=32.33 Å [1, 18, 19]. According to Gödecke and Schubert [15], for the tetragonal β-In_2S_3 the maximum amount of indium should be below 40.5 at% (Fig. 1.1 a).
   - The cubic α-In_2S_3 with the space group of $Fd\bar{3}m$ exists from 414 °C up to 750 °C. The cubic In_2S_3 with the lattice parameters of a=b=c=10.77 Å crystallizes in a defect spinel structure in which one third of tetrahedral disordered cationic sites remain empty [1, 20, 21]. According to Gödecke and Schubert [15], α-In_2S_3 forms in the systems with indium content above 40.5 at.% at room temperature.
   - The trigonal γ-In_2S_3 with the space group $P\bar{3}ml$ and with the lattice parameters a=b=6.56 Å and c=17.57 Å exists at temperatures higher than 750 °C up to the melting point of In_2S_3 at 1090 °C [22 – 24]. The layered structure of high-temperature γ-In_2S_3 can be described as random distribution of only octahedrally coordinated cation atoms [22].

In spite of intense research, there is notable confusion concerning the labeling of different crystalline modifications of In_2S_3 [14, 16, 23]. For example, Diehl and Nitsche [23] labeled the tetragonal In_2S_3 with the space group of $I4_1/amd$ as "β-In_2S_3". Later Massalski et al. [16] published the phase diagram for the In-S system (Fig. 1.1 b), where the In_2S_3 with the same space group was labeled as "α-In_2S_3", and the cubic modification was labeled as "β-In_2S_3". In my thesis the tetragonal In_2S_3 with the space group of $I4_1/amd$ will be labeled as "β-In_2S_3", as accepted by majority of authors [1, 14, 15].

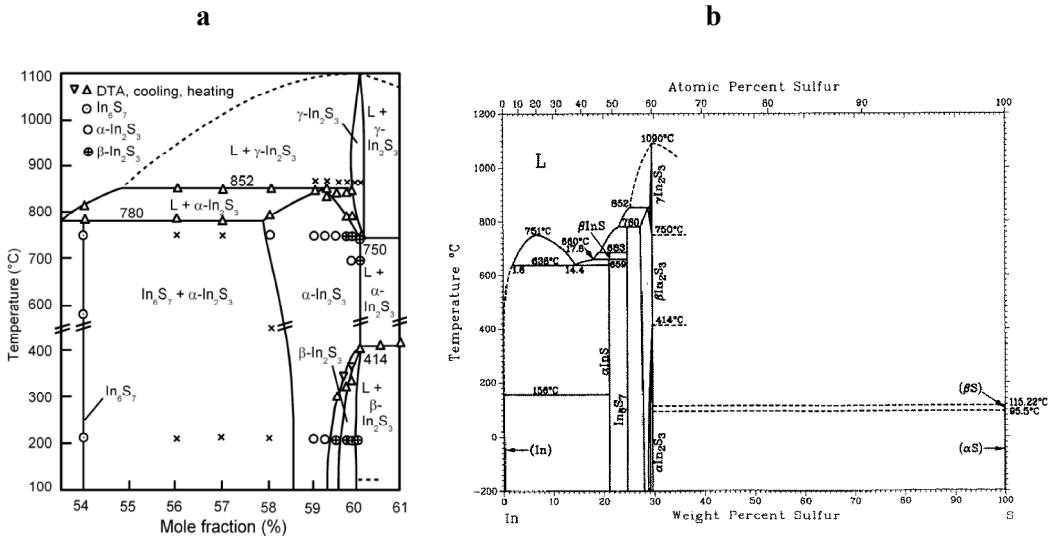

Fig. 1.1. a – The fragment of the phase diagram of the In-S system by Gödecke et al. [15] and b – the entire phase diagram of the In-S system according to Massalski et al. [16], where labels for "β-In_2S_3" and "α-In_2S_3" are exchanged.

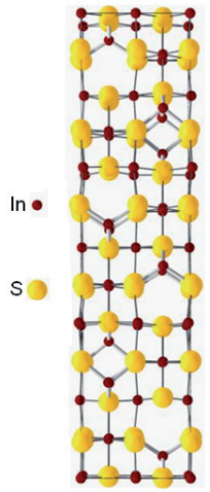

Fig. 1.2. Crystal structure of tetragonal β-In_2S_3 [14].

For β-In_2S_3 single crystal the direct optical bandgap of ~2.0 eV has been reported by Rehwald and Harbeke [18] and Kambas et al. [25], while an indirect bandgap of 1.98 eV has been determined by Nakanishi et al. [26]. Markedly higher bandgap values of 2.24 eV and 2.64 eV for indirect and direct transitions, respectively, have been found for β-In_2S_3 single crystal by Choe et al. [27]. Thus, there is no agreement in the literature whether β-In_2S_3 single crystals have direct or indirect or both optical transitions.

Electrical properties of β-In_2S_3 single crystals were comprehensively studied by Rehwald et al. [18] and the n-type conductivity has been determined for the

β-In_2S_3 single crystals. It has been found that a lack of sulfur compared to the stoichiometric In_2S_3 increases the electron density, i.e. increases the n-type character; however the crystals with sulfur excess did not change the sign of the charge carriers [18].

Besides applications in the manufacturing of optoelectronic devices (detailed discussion below), In_2S_3 has been also used as a photocatalyst e.g. for the photodegradation of toxic and harmful chemical substances [28, 29]; for manufacturing hydrogen from water-containing organic sludge [30]. In_2S_3 has been applied as one of the components for making modified germanium sulfide glass with improved mechanical and optical properties such as extended transmission in the infrared spectral region and the glass transition temperature in the range of 370 – 550 °C with the thermal stability in the region of 100 – 300 °C [31].

1.2 In_2S_3 thin films

Deposition methods and properties of In_2S_3 films deposited by different methods

In_2S_3 thin films can be obtained by different physical and chemical methods. Main physical methods for the preparation of In_2S_3 films are physical vapor deposition (PVD) [32, 33] and sputtering [34, 35]. Chemical methods are atomic layer deposition (ALD) [36, 37], chemical bath deposition (CBD) [32, 38 – 41], spray ion layer gas reaction (Spray-ILGAR) [42], spin coating [43], successive ionic layer adsorption and reaction (SILAR) [44, 45], chemical spray pyrolysis (CSP) [2, 46 – 49]. Chemical composition, crystalline and optical properties of the In_2S_3 films depend strongly on the used deposition method [1].

Mostly amorphous In_2S_3 films have been obtained, when substrate or process temperatures are below ~150 °C. Then the post deposition annealing has been used to obtain crystalline β-In_2S_3 films [33, 43, 45 50]. The crystalline β-In_2S_3 films can be obtained with most of the deposition methods (without applying the post treatment methods), where substrate or process temperatures are over ~150 °C [32, 36, 38].

The transition type of In_2S_3 thin films is a subject of discussion in the literature, with no agreement on whether the transition is a direct or an indirect allowed transition [1, 51]. The optical bandgap values of β-In_2S_3 films obtained by different methods vary in a wide range from 2.0 eV up to 3.7 eV for direct transition [1]. The direct bandgap values of the PVD grown films were between 2.0 eV and 2.3 eV [20, 33, 52 – 55]. While Allsop et al. [42] assumed indirect transition in In_2S_3, and reported the bandgap value of 2.2 eV for the films obtained by Spray-ILGAR process. For In_2S_3 films, deposited with similar precursors ($In(CH_3COCHCOCH_3)_3$ and H_2S) and deposition temperatures (160 – 180 °C) by ALD, Naghavi et al. [36] determined the direct bandgap value of about 2.7 eV, but Sterner et al. [56] reported indirect bandgap value of 2.08 eV. Asikainen et al. [57] determined the direct bandgap of 2.3 eV for the ALD-In_2S_3 films deposited at higher deposition temperatures (300 – 400 °C) by using $InCl_3$ and H_2S. In_2S_3 films deposited by CBD have the widest range of direct bandgap values from 2.3 – 3.7 eV [41, 58, 59]. The

wide bandgap range of CBD deposited films is due to the strong effect of the different chemical bath properties (e.g. pH, bath temperature) [58].

In_2S_3 films deposited by the wet-methods such as ILGAR [42], CSP [47, 60] and CBD [61, 62], contain a variable amount of oxygen or chlorine (depending on the used precursor solution and deposition temperature). It has been found that different impurities, such as sodium [63], oxygen [64] or copper [65] in the In_2S_3 thin films influence the bandgap values. Impurities, such as sodium and oxygen in the In_2S_3 films have been found to increase the bandgap values from 2.1 eV up to ca. 2.9 eV (for direct transitions) with increasing impurity concentrations [63, 66]. When copper was incorporated into the film (at an atomic ratio of Cu:In of 0.2), the bandgap decreased down to 1.55 eV [65], presumably due to the fact that $CuInS_2$ was formed. In_2S_3 films with the minimum amount of contamination with foreign elements can be obtained by using the PVD process such as evaporation [34].

In_2S_3 thin films have been reported to be n-type, with high resistivity values [36, 54]. For a 300 nm thick ALD-In_2S_3, Asikainen et al. [57] found the resistivity to be about $2 \cdot 10^7$ Ω cm (after exposing to daylight). For In_2S_3 films deposited by CBD, the resistivity values of 10^7 to 10^8 Ω cm have been reported by Bayón et al. [59].

Application of In_2S_3 thin films

In_2S_3 thin films obtained by different methods have been applied for optoelectronic applications due to their stability, wide bandgap and suitable transmittance in the visible spectrum region [3, 4, 48, 67, 68]. In photovoltaic structures, In_2S_3 thin films have been used as a buffer layer in $Cu(In,Ga)(S,Se)_2$ based solar cells instead of cadmium sulfide (CdS). The efficiencies of $Cu(In,Ga)(S,Se)_2$ absorber based solar cells with In_2S_3 buffer layer deposited by different methods are presented in Table 1.1. It can be seen that the highest efficiency of 16.4% has been achieved by using the ALD-In_2S_3 buffer layer [69]. Lately, a solar cell with the efficiency of 16.1% has been obtained by using ILGAR-In_2S_3 as buffer layer [70]. In chalcopyrite absorber layer based solar cells the main roles of the buffer layer are [14]:

- to be n-type for the carrier separation;
- to match the lattice parameters between the absorber and the window layer;
- the buffer material band structure must fit with the band structure of the absorber material to reduce carrier recombination at absorber/buffer heterointerface.

In_2S_3 film has also been used as an absorber in ETA-type nanostructured solar cell based on ZnO nanorods [73, 74]. The thickness of the absorber should be extremely thin (10 up to 30 nm) in an ETA cell [73]. Recently In_2S_3 has been proposed as a candidate for host material of an absorber in two-photon absorption processes based solar cells (also called as intermediate band solar cells) [5, 6]. In intermediate band solar cells, in the absorber multiple energy levels are used to absorb different wavelengths of the solar spectrum. This means that one or more energy levels within the bandgap of the absorber absorb photons in parallel with the

normal operation of a single bandgap cell. It has been proposed that transition metals (TM) such as titanium or vanadium seem to be appropriate dopants to make an intermediate band material [5].

Table 1.1 Efficiencies for $Cu(In,Ga)(S,Se)_2$ solar cells with In_2S_3 buffer layer (and CdS with maximum efficiency for comparison) as a buffer layer

Buffer layer	Method	$T_{substrate}$, °C	Annealing, °C	Efficiency, %	Reference
CdS	CBD	60	-	19.9	71
In_2S_3	ALD	220	-	16.4	69
In_2S_3	ILGAR	220	-	16.1	70
In_2S_3	CBD	70	200	15.7	62
In_2S_3	PVD	<50	200	15.2	72
In_2S_3	Sputtering	220	-	13.3	4
In_2S_3	USP	200	-	12.4	2

In summary, despite of differences in the reported optical band gap values and chemical composition, In_2S_3 thin films made by various methods are suitable buffer layers for high efficiency thin film solar cells based on $Cu(In,Ga)Se_2$ absorbers (Table 1.1) [35, 68]. Moreover, tetragonal In_2S_3 could be used as absorber material in two-photon absorption processes based solar cells [5].

1.3 Chemical spray pyrolysis method

Chemical spray pyrolysis (CSP) is a low-cost, simple, non-vacuum method for deposition of large area thin films with relatively low production cost and technological abilities for mass production [75 – 77]. The first paper about CSP was published by Chamberlin and Skarman in 1966 on the preparation of CdS films [78]. Since then the CSP method has been used to deposit a variety of thin films, such as different metal sulfides e.g. CdS, ZnS, SnS, Cu_xS, $CuInS_2$ [7, 13, 79 – 86] and metal oxides, such as CdO, ZnO, TiO_2 SnO_2, MgO [87 – 94], which are used in many devices like solar cells, sensors, solid oxide fuel cells and other devices.

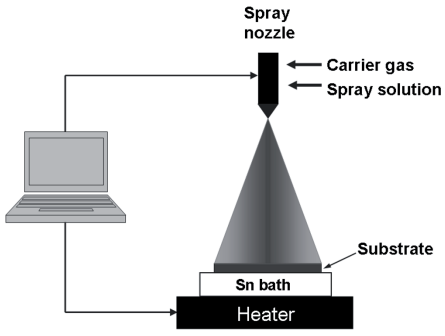

Fig. 1.3. The scheme of the spray pyrolysis set-up.

In the CSP process aqueous or alcoholic solution of precursor chemicals is pulverized in the form of fine droplets to the preheated substrate where thin film is formed (Fig. 1.3). The CSP equipment set-up consists of an atomizer, which generates very fine droplets of a precursor solution, a substrate heater, a temperature controller and a solution container [78, 79]. CSP techniques can be divided into pneumatic, ultrasonic and electrostatic spray modes depending on the method of generating microsized droplets (atomization) of the precursor solution. In the pneumatic CSP mode the droplets of the precursor solution, generated by the atomizer are sprayed with the help of the carrier gas onto the preheated substrate. In the ultrasonic CSP mode the solution droplets generated with the help of an ultrasonic actuator with smaller size and are pulverized with much lower velocity [95] compared to that by the pneumatic CSP. In the electrostatic CSP mode the fine (in submicrometers), uniform, self-dispersive (nonagglomerated) droplets are sprayed with the help of high electrical field applied between spray nozzle and substrate [96 – 97].

The disadvantages of the CSP [79, 98] are related to the difficulties with precise surface temperature determination during the film deposition process, the three-dimensional growth mechanism of the film and the limited number of precursors for different film, because the precursor salts must be soluble in the used solvent.

Despite these disadvantages, different metal oxide films have been successfully made by CSP [76, 99, 92]. Metal sulfide films with device quality can also be deposited by CSP, however due to an open system the unwanted oxidation can take place during the film growth [12, 100 – 103].

The pneumatic CSP method has been used by the researchers at TUT to deposit different thin films, starting from the studies by Dr. K. Kerm on the deposition of CdS thin films in the 1970s [7]. Since then CSP equipment has been significantly improved and the ongoing depositions of different metal sulfide (ZnS, $CuInS_2$, CdS, In_2S_3) and metal oxide (TiO_2, ZnO) films have been performed by the research group led by Dr. M. Krunks [8 – 10, 104, 105]. This work continues the above studies, expanding the list of the metal sulfides with a comprehensive study on deposition of In_2S_3 films by CSP.

1.4 Different metal sulfides by CSP

CSP method has been used to deposit a variety metal sulfide thin films, such as CdS (the films have been used in solar cells, optical detectors) [13, 86, 107]; ZnS (the films used in sensors, lasers, ultraviolet-light-emitting diodes and other devices) [80, 81, 104, 108], SnS (the films have been mainly used in solar cells) [82,100, 109]; Cu_xS (the films used in solar cells, electroconductive coatings and other devices) [83, 110, 111], $CuInS_2$ (the films used mainly in solar cells) [112 – 115].

Generally, the spray solution containing metal chloride (with or without hydrate) and sulfur source (usually thiourea) as starting chemicals are used to deposit the metal sulfide film by CSP [76, 83, 112, 100, 116]. The main technological parameters influencing the properties of CSP deposited metal sulfide

films are the growth temperature and the molar ratio of the precursor chemicals in the spray solution. In addition to these two main parameters the properties of spayed films depend also on the used precursor chemicals, growth environment, the substrate properties, the used solvent, spray set-up and on other aspects [77, 79]. For example, ZnS film deposited at 600 °C from an aqueous solution containing $ZnCl_2$ and $SC(NH_2)_2$ at the Zn:S molar ratio of 1:1 by CSP in addition to the main ZnS phase, contained a crystalline ZnO phase [104]. ZnS film deposited also at 600 °C, but with Zn to S precursors molar ratio of 1:2 in the spray solution, did not contain the ZnO phase [104]. On the other hand, the ZnS films with poor crystallinity were deposited below 400 °C, irrespective of the molar ratio of the Zn to S in the aqueous spray solution [104]. As a result it was found that closely stoichiometric ZnS films can be grown at 500 – 600 °C in air using spray solution containing $ZnCl_2 : SC(NH_2)_2 = 1:2$ (molar ratio) [104]. To explain and understand these results, the formation of metal sulfide in CSP should be investigated.

Formation of different metal sulfides in the CSP process

Many studies have been reported on the formation of various metal sulfides (where metal is Cd, Zn, Cu or Sn) in the CSP process [116 – 124]. These studies include synthesis and characterization of different compounds formed in the spray solution, their structure and thermal degradation in an inert and oxidative atmospheres. It has been found that many metal halogenides and thiourea in an aqueous spray solution form different complex compounds with different stoichiometries [117, 124]. According to the studies, in complex compounds the thiourea ligand is coordinated through sulfur atoms to the metal (Cu(I), Zn(II), Cd(II), Sn(II)) cations [116, 118, 125 – 127]. These complex compounds can be presented with general formula $Me_m(tu)_nX_o$ or $Me_m(tu)_nX_o \cdot yH_2O$, where Me is a metal (Cd, Zn, Cu or Sn), m is a number of metal atoms forming the complex compound, tu is $SC(NH_2)_2$, X is halogen (Cl, Br), n is a number of ligand molecules coordinatively bonded to metal cation, y is a number of water molecules and o is a number of halogen anions [117 – 126]. These different complex compounds upon their thermal decomposition lead to the formation of metal sulfides.

The formation of various complex compounds with different stoichiometries is determined by the molar ratio of the starting chemicals, pH of the solution and the coordination number of the metal [116, 125]. For example, $CuCl_2$ and $SC(NH_2)_2$ (tu) at molar ratios of 1:1 and 1:2 form the complex compound $Cu_2(tu)_2Cl_2 \cdot H_2O$ [9, 121]. When CuCl and tu have been taken at molar ratios of 1:1 and 1:3 the obtained complex compounds were $Cu_2(tu)_2Cl_2 \cdot H_2O$ and $Cu_2(tu)_6Cl_2 \cdot 2H_2O$, respectively [120, 125]. Similarly, by taking CuBr and tu at molar ratios of 1:1 and 1:3 the obtained complex compounds were $Cu_2(tu)_2Br_2 \cdot H_2O$ and $Cu_2(tu)_6Br_2 \cdot 2H_2O$, respectively [125].

To determine basic reactions occurring during the thermal degradation of these different metal-thiourea complex compounds the thermoanalytical studies have been conducted by simultaneous TG/DTA/EGA techniques in inert and in air atmospheres [116 – 124]. It has been found that thermal decomposition of metal-thiourea complex compounds (where metal is Cd, Zn, Cu or Sn) is a complicated

multistep process. The thermal decomposition of all studied metal–thiourea complex compounds in inert atmosphere involved only endothermic processes [118 – 121]. The thermal decomposition of metal-thiourea complex compounds in air shows the endothermic and exothermic effects [116 – 118, 121, 122]. To find out the reactions occurring during the thermal decomposition the solid decomposition products and gaseous species evolved during the decomposition step have been studied. *Ex situ* XRD and FTIR studies have been applied to characterize the solid products of thermal decomposition. Gaseous species evolved in each step were determined applying the methods of EGA-FTIR and EGA-MS. Generally, the metal halogenide-thiourea complexes (where metal is Cd, Zn, Cu or Sn) are thermally stable up to ca. 200°C, they decompose at temperatures slightly above 200 °C and form metal sulfides upon decomposition around 230 – 250 °C, irrespective of the atmosphere. Commonly, metal sulfides are the final decomposition products in an inert atmosphere above 500 °C; however, in oxidative atmospheres metal oxides are the final products [117, 119 – 121, 128]. The evolved gaseous species include NH_3 (ammonia), HCl (hydrogen chloride), CS_2 (carbon disulfide), H_2NCN (cyanamide), HNCS (isothiocyanic acid), HCN (hydrogen cyanide), SO_2 (sulfur dioxide), COS (carbonyl sulfide) and CO_2 (carbon dioxide) in air while in an inert atmosphere NH_3, HCl, CS_2, H_2NCN and HNCS are the main gases evolved [118, 121, 122]. For example, formation of CdS from a complex compound $Cd(tu)_2Cl_2$ has been investigated by using both TG/DTA/EGA-FTIR and *ex situ* XRD studies [118]. The evolution of H_2NCN and HNCS were detected by TG/EGA-FTIR, when the complex compound of $Cd(SC(NH_2)_2)_2Cl_2$ was heated up to 250 °C. Hence, from the solid residues heated up to 250 °C the presence of crystalline NH_4CdCl_3 (ammonium cadmium trichloride) in addition to CdS was detected by *ex situ* XRD. According to the results from thermal decomposition and XRD studies the formation of CdS could be presented as Eqs. 1.1, 1.2 [118]:

$$3CdCl_2+SC(NH_2)_2+2NH_3 \rightarrow CdS+2NH_4CdCl_3+H_2NCN \quad (1.1)$$

$$3CdCl_2+CS_2+3NH_3 \rightarrow CdS+2NH_4CdCl_3+HNCS \quad (1.2)$$

The formation of zinc ammonium chloride or ammonium copper chloride was not observed during the thermal decomposition of $Zn(tu)_2Cl_2$ and $Cu_2(tu)_6Cl_2{\cdot}2H_2O$ complex compounds, respectively [119, 120].

The thermal decomposition of metal-thiourea (Cu(I), Zn(II), Cd(II)) complexes were similar up to 300 °C in air, but at higher temperatures differences between different metal-thiourea complexes occurred. It was observed that final exothermic decomposition reactions of the $Cu_2(tu)_6Cl_2{\cdot}2H_2O$ complex take place at lower temperature regions (350 – 450 °C) than in the case of $Zn(tu)_2Cl_2$ and $Cd(tu)_2Cl_2$ complexes, where final exothermic processes occurred at around 700 °C [118 119, 121, 122].

The thermal decomposition of the different metal (Zn(II), Cd(II)) chloride – thiourea complex compounds in the air were finished at lower temperature than the thermal decomposition carried out in the inert atmosphere. For example, a final product of the thermal decomposition of the complex $Zn(tu)_2Cl_2$ was ZnO in air at 770 °C, while in the inert atmosphere the final product was ZnS at around 900 °C [119].

In summary, to understand the chemistry leading to the formation of the metal sulfides by CSP, simultaneous thermoanalytical methods (TG/DTA and TG-EGA) and *ex situ* XRD and FTIR have been applied to study the thermal decomposition of complex compounds formed in the spray solution. The temperature of the thermal decomposition of the complex compound determines the lowest temperature at which metal sulfides can be deposited by CSP. The reactions occurring during the thermal degradation provide information of the different foreign phases in the film. As a result, it was found that CuS and SnS_2 thin films should be deposited at much lower temperatures (up to 270 °C) than CdS and ZnS films (around 450 °C) to reduce the unwanted oxidation processes during deposition of these thin films by CSP [119, 128].

1.5 In_2S_3 thin films by CSP

Effect of indium source and molar ratio of starting chemicals in the spray solution on the film properties

Aqueous or alcoholic solutions containing indium chloride ($InCl_3$) and thiourea ($SC(NH_2)_2$, tu) have been generally used for In_2S_3 thin films deposition by CSP [2, 46, 47]. When $InCl_3$ was used as indium source, chlorine residues were found throughout the In_2S_3 films grown around 300 °C [47]. Nitrate ($In(NO_3)_3$) [129] or acetate based ($In(CH_3COO)_3$) [48] solutions have been used to avoid the chlorine contamination in the films. However, In_2S_3 films obtained by using nitrate or acetate based precursors were amorphous at growth temperatures of 300 °C [48, 129].

It has been found that the molar ratio of the $InCl_3$ and $SC(NH_2)_2$ in the spray solution has an effect on the crystallinity, the crystallite size [2, 48], and the optical bandgap of the In_2S_3 films [46, 47, 129]. Kim et al. [46] found that indirect bandgap values of sprayed films deposited at 350 °C increased (from 2.15 up to 2.43 eV) by increasing the thiourea concentration in the spray solution [46]. In contrast, John et al. [47] reported the decrease in direct bandgap values from 2.81 to 2.64 eV, when the molar concentration of thiourea in the spray solution was increased ($InCl_3$: $SC(NH_2)_2$ = 2:1 up to 1:4 (molar ratio)) for the films deposited at 300 °C.

According to the XPS study by John et al. [47], the presence of oxygen was detected through the In_2S_3 films deposited at 300 °C by using the $InCl_3$: $SC(NH_2)_2$ = 1:1 (molar ratio). Presence of oxygen has been confirmed by the O1s core level peak located in the binding energy (BE) region of 531.5–532.6 eV in the XPS spectrum in addition to the S2p peak at BE=166.9 eV. They explained the presence of oxygen due to the formation of a mixed phase of indium sulfate and sulfite, in addition to the indium sulfide phase [47]. In_2S_3 films with no oxygen inside have been deposited at 300 °C by using $InCl_3$: $SC(NH_2)_2$ = 1:4 (molar ratio) in the spray solution [47]. Interestingly, oxygen (11 at%) bounded to indium (O1s peak at BE = 530.3 eV) has been detected in the film deposited at 340 °C by using $InCl_3$: $SC(NH_2)_2$ = 1:2 (molar ratio) in the spray solution [103].

Influence of growth temperature on the film properties

The growth temperature has been found to control the crystal structure, the crystallite size, film thickness and optical properties of In_2S_3 [2, 46 – 49]. Calixto-Rodriguez et al. [48] reported that increasing the growth temperature (≥400 °C) leads to films with better crystallinity. The chlorine concentration in the film decreases with the increase of the deposition temperature (180 – 290 °C) [131]. A decrease in the film thickness with increasing growth temperature is a phenomenon characteristic of spray-deposited films [11]. However, Ernits et al. [49] reported the increase in the In_xS_y films thickness with increasing the deposition temperature by using the solution containing $InCl_3$: $SC(NH_2)_2$ with molar ratio of 1:3. The In_xS_y films deposited at substrate temperature of 310 and 380 °C exhibited the thickness of 35 and 120 nm, respectively and transparency of 97 and 84 %, respectively [49]. John et al. [47] reported a decrease in direct optical bandgap values (from 2.67 to 2.58 eV) increasing the growth temperature from 300 up to 380 °C for the films deposited with $InCl_3$:$SC(NH_2)_2$ molar ratio of 2:3 in the spray solution.

In general, crystalline β-In_2S_3 thin films can be obtained with aqueous or alcoholic solutions containing $InCl_3$ and $SC(NH_2)_2$ by using pneumatic or ultrasonic CSP. The spray solutions with an excess of sulfur source (from at least $InCl_3$: $SC(NH_2)_2$ = 2:3, molar ratio) and the growth temperatures in the range of 200 – 300 °C have been used to obtain β-In_2S_3 thin films [2, 46, 47, 49, 103, 130]. Moreover, the increased sulfur source concentration in the spray solution decreased oxygen and chlorine concentrations in the films [2, 131]. On the other hand, also the increase in the growth temperature decreases the impurity content (e.g. chlorine contamination) in the sprayed In_2S_3 thin films [2, 131]. In_2S_3 films with low crystallinity and high impurity concentrations have been obtained when spray solution with an excess of indium source ($InCl_3$: $SC(NH_2)_2$ = 2:1 and 1:1, molar ratio) at growth temperatures below 400 °C have been used. [2, 47, 131].

Formation of In_2S_3 in the CSP process

No comprehensive studies of the formation of In_2S_3 in the CSP process by using aqueous spray solutions containing $InCl_3$ and $SC(NH_2)_2$ have been reported. Kumar et al. [132] described the formation of In_2S_3 in the spray process by the following reaction (Eq. 1.3):

$$2InCl_3+3CS(NH_2)_2+6H_2O \rightarrow In_2S_3+3CO_2+6NH_4Cl \qquad (1.3)$$

This general reaction is too simple in the light of the results of studies performed on the formation of other metal sulfides such as CdS, ZnS, SnS and Cu_xS in the spray pyrolysis process [116 – 124]. Moreover, this general reaction (Eq. 1.3) has not been experimentally confirmed.

In addition, probable interaction of $InCl_3$ and thiourea in the spray solution is neglected although neutral sulfur-based donors, such as thiourea (and thioether) could form adducts with indium(III) ions [133]. It is reported that In(III) halides (InX_3, where X is halogen) can form different complex compounds with general

formula of InX_3L, InX_3L_2 and InX_3L_3, where L is a ligand [133]. One of these known structures is the complex compound trichlorobis(N,N,N',N'-tetramethylthiourea)indium(III) representing the $InCl_3L_2$ type complex, where L is N,N,N',N'-tetramethylthiourea [134]. It is also known that thiourea and $[In(H_2O)_6](ClO_4)_3$ form a complex compound $[In(tu)_6](ClO_4)_3$ [135]. Malyarik et al. [136] described the formation of $In(tu)_3Cl_3$ in an aqueous solution containing $InCl_3$ and thiourea at molar ratios of 1:1 and 1:3.

The thermal analysis has been performed for $[InCl_3(tu)_4]$, the compound obtained by mixing $InCl_3$ and thiourea [137]. Whereas Indium (In^{3+}) coordination number is 4, 5 or 6 [133], the formation of the latter complex is questionable. Moreover, no details of the preparation of this compound have been reported. The thermal analysis has been described only in general terms, the decomposition temperatures and the mass loss steps were not indicated. According to the differential scanning calorimetry (DSC) curve during the thermal decomposition of $[InCl_3(tu)_4]$, the endothermic peaks and one exothermic peak have been observed in argon atmosphere [137], however the reason of this exothermic effect detected in inert atmosphere has not been explained. According to the thermal analysis of $[InCl_3(tu)_4]$, it was proposed that thiourea was lost in the first two mass loss steps followed by the decomposition of $InCl_3$ in a third mass loss step [137]. Unfortunately, Dunstan [137] did not present the experimantal data confirming the formation of $[InCl_3(tu)_4]$, neither the compound decomposition temperature, nor the final decomposition product were determined.

According to the literature survey, only few studies cover the formation of complex compounds in the InX_3- thiourea system. To our best knowledge, the formation of In_2S_3 during the CSP process when using $InCl_3$ and thiourea as starting chemicals has not been studied.

1.6 Summary of the literature review and aim of the study

From the literature review on In_2S_3 films it can be summarized as follows:

1. In_2S_3 thin films have been generally applied for optoelectronic applications due to their stability, wide bandgap and suitable transmittance in the visible spectrum region. In photovoltaic structures, In_2S_3 thin films have been used as a buffer layer in $Cu(In,Ga)(S,Se)_2$ based solar cells instead of CdS. In_2S_3 thin films as buffer layers in solar cells can be prepared by various methods. Recently it was suggested that tetragonal In_2S_3 could be used as an absorber material in two-photon absorption processes based solar cells.
2. Chemical spray pyrolysis has been chosen for the deposition of different metal oxide and metal sulfide thin films because it is a simple non-vacuum method, which requires short processing time for large area thin film deposition, with relatively low production costs.
3. Aqueous or alcoholic solutions containing $InCl_3$ and $SC(NH_2)_2$ have been mainly used for the deposition of In_2S_3 thin films by pneumatic or ultrasonic CSP.

4. It has been found that the molar ratio of indium and sulfur sources in the spray solution and the growth temperature are the main parameters controlling the phase and chemical composition, structure, and optical properties of the sprayed In_2S_3 film.
   - *Effect of the film growth temperature:*
     In general, crystalline β-In_2S_3 films can be obtained by spraying of aqueous or alcoholic solutions containing $InCl_3$ and $SC(NH_2)_2$ in the temperature range of 200 – 300 °C. The increase in the growth temperature has been found to decrease the chlorine content and increase the crystallite size in the sprayed In_2S_3 thin films. The influence of film growth temperature on the content of oxygen in the thin film has not been studied. The lowest possible temperature for the deposition of In_2S_3 thin films is undefined.
   - *Effect of the starting chemicals molar ratio in the solution:*
     The presence of oxygen containing products has been detected in the In_2S_3 films deposited at around 300 °C using aqueous spray solutions with the $InCl_3$: $SC(NH_2)_2$ molar ratios of 1:1 and 1:2. Deposition at a similar temperature using a higher content of thiourea in the solution reduces the content of oxygen in the sprayed In_2S_3 film. The bandgap values have been found to increase with increasing the concentration of thiourea ($InCl_3$: $SC(NH_2)_2$ = 2:1 up to 1:4 (molar ratio)) in the spray solution for the films deposited at 300 °C. Reasons explaining the effect of starting chemicals molar ratio on the film properties have not been reported in literature.
5. To our best knowledge, no systematic study on the effect of the growth temperature and the molar ratio of the starting chemicals ($InCl_3$ and $SC(NH_2)_2$) in the aqueous or alcoholic spray solution on the phase and elemental composition, structural, morphological and optical properties of In_2S_3 films deposited on the same set-up has been performed. Different research groups have used various CSP set-ups, which makes it difficult to compare the results obtained.
6. No comprehensive studies on the formation mechanism of In_2S_3 in the CSP process have been reported. In the literature, only one reaction has been proposed for the formation of In_2S_3 in the CSP process [132]. This general reaction has not been experimentally confirmed. Moreover, this reaction is too simple compared to the formation of other metal sulfides (e.g. CdS, SnS, ZnS, Cu_xS) in the CSP process using metal halogenides and thiourea as starting chemicals. Halogenides of Cd, Zn, Sn and Cu and thiourea form complex compounds with different stoichiometries in an aqueous solution. Metal sulfides form upon thermal decomposition of metal halogenide thiourea complexes.

Based on the above conclusions, the objectives of this doctoral thesis were:

- To study the influence of $InCl_3$ to $SC(NH_2)_2$ molar ratio in an aqueous or alcoholic spray solution and the growth temperature on the phase and elemental composition, and the structural and optical properties of In_2S_3 films deposited by pneumatic CSP.

- To understand the formation of In_2S_3 films in the CSP process using $InCl_3$ and $SC(NH_2)_2$ as starting chemicals:

    - To study the precursors for sprayed In_2S_3 films which are formed in an aqueous spray solution using $InCl_3$ and $SC(NH_2)_2$ as indium and sulfur sources, respectively, at molar ratios of 1:3 and 1:6.

    - To study the thermal decomposition process of the precursors for In_2S_3 films by means of simultaneous thermogravimetric and differential thermal analysis coupled online with evolved gas analyses and applying *ex situ* XRD and FTIR studies for solid products.

2. EXPERIMENTAL

The experimental can be divided into two main parts. The first part describes in detail the preparation and characterization of In_2S_3 thin films deposited by the pneumatic CSP method. The second part is focused on the studies of formation chemistry of In_2S_3 in the CSP process, and covers the synthesis, characterization and thermal analysis of single-source precursors for the In_2S_3 films by CSP. General description of the experiment is summarized briefly in the following section. The experimental details are presented in publications [**I** – **IV**].

2.1 CSP deposited In_2S_3 thin films

2.1.1 Preparation of In_2S_3 thin films

In_2S_3 thin films were prepared by the pneumatic CSP method using compressed air as carrier gas. The the aqueous and alcoholic solutions solutions used for the study contained indium(III)chloride ($InCl_3$) and thiourea ($SC(NH_2)_2$) (p.a.>98%, Merck-Schnchardt S32896) at molar ratios (In:S) of 1:3 and 1:6 whereby keeping the concentration of $InCl_3$ constant at $[In^{3+}] = 2\times10^{-3}$ mol/l. To prepare the InCl3 solution, indium wire (p.a. 99.99%, Alfa Aesar) was dissolved in concentrated hot hydrochloric acid (HCl) from Merck. For aqueous solutions the deionized water was used as a solvent. The mixture of H_2O and ethanol (H_2O:C_2H_5OH =1:1, by volume) or H_2O and isopropyl alcohol (H_2O:C_3H_7OH =1:1, by volume) as the solvents was used for alcoholic solutions [**II**]. Microscopy glass slides with a size of $20\times20\times1.1$ mm^3 were used as substrates. In the case of the films deposited using H_2O as a solvent, growth temperatures (T_s) were varied from 205 to 410°C. T_s was measured at various temperatures from the glass surface placed on the tin bath, when deionized water was sprayed [**I**]. The alcoholic solutions were deposited at tin bath temperatures (T_{Sn}) of 250 and 330 °C [**II**]. Total volume of the solution sprayed was 50 ml and the rate of spray was 2.5 ml/min in all runs. The scheme of the spray pyrolysis set-up used in this study is presented in paper [**I**].

2.1.2 Characterization of In_2S_3 thin films

The phase composition, morphology, elemental composition and optical properties of CSP deposited In_2S_3 thin films were determined by the characterization methods summarized briefly in Table 2.1.

Table 2.1. Methods used for the characterization of In_2S_3 thin films

Properties	Characterization method	Apparatus	Ref.
Phase composition, orientation of crystallites, crystallite size	XRD	Rigaku Ultima IV	[**I**, **II**]
Morphology, thickness, grain size	SEM	Zeiss HR FESEM Ultra 55 EVO-MA15	[**I**, **II**] [**I**]
Elemental composition	EDX	Röntec EDX XFlash 3001 detector Oxford Instruments INCA Energy system	[**I**] [**I**]
	XPS	Kratos AXIS Ultra DLD	[**I**, **II**]
Optical absorption, transmission, bandgap	UV-VIS spectroscopy	Jasco V-670	[**I**, **II**]

2.2 Synthesis and characterization of precursors for sprayed In_2S_3 films

2.2.1 Preparation of the precursors

To characterize the precursor materials for sprayed In_2S_3 films using $InCl_3$ and thiourea as starting chemicals, the aqueous solutions containing 0.1 M $InCl_3$ and 0.75 M $SC(NH_2)_2$ were mixed at two different $InCl_3$ (In) to thiourea (S) molar ratios of 1:3 (named as **1**) or 1:6 (named as **2**) at room temperature. In both cases, indium concentration, $[In^{3+}]$, was $5 \cdot 10^{-2}$ mol/l. The solutions were left to evaporate slowly at 50 °C in a thermostat for a week. The obtained dried powders **1** and **2** were characterized with respect to the elemental composition, structure and used for thermal analysis [**III** and **IV**].

2.2.2 Characterization of precursors

Table 2.2 summarizes the analytical techniques used for the characterization of samples **1** and **2** as precursors for In_2S_3 films deposition by CSP, details of the analytical methods applied are given in papers [**III**] and [**IV**].

Table 2.2 Methods used for the characterization of precursors for In_2S_3 films

Properties	Characteri-zation method	Apparatus	Ref.
Structure	FTIR	Perkin-Elmer GX1	[**III**]
Crystallinity, phase composition	XRD	Rigaku Ultima IV X'pert Pro MPD	[**III**] [**IV**]
Elemental composition	Elemental analysis of C, N, H Cl	Gmbh Vario EL CHNOS Vario ELIII CHN Amperometric titration	[**III**] [**IV**] [**III**]
Structure of single crystal	XRD	Rigaku R-AXIS IV++ image plate diffractometer	[**IV**]
Thermal decomposition (temperatures, type of reactions (endo/exo), gases evolved)	TG/DTG/DTA	SetSys-Evolution TGA 2050 STD 2960	[**III**] [**IV**] [**IV**]
	TG/EGA-FTIR TG/EGA-MS	SetSys-Evolution +Nicolet 380 TGA 2050 +BioRad TGA-IR STD 2960+ThermoStar GDS 300 T3	[**III**] [**IV**] [**IV**]

3 RESULTS AND DISCUSSION

3.1 In_2S_3 films by CSP

The influence of different deposition parameters on the properties of In_2S_3 thin films deposited by the pneumatic CSP method is summarized in this subsection. In_2S_3 films were deposited from aqueous [**I**, **II**] and alcoholic [**II**] spray solutions containing $InCl_3$ and $SC(NH_2)_2$ with the molar ratio of 1:3 and 1:6 (hereinafter abbreviation "In : S" is used for $[InCl_3]$:$[SC(NH_2)_2]$). The effect of different growth temperatures and precursors molar ratios in solution on the structural and optical properties, as well as on the composition and morphology of sprayed In_2S_3 thin films was studied. Results of the studies are presented in papers [**I**] and [**II**].

The substrate temperature (T_s) represents the film growth temperature in publication [**I**]. In publication [**II**] we operated with the tin bath temperatures (T_{Sn}). For better comparison of the results presented in [**I**] and [**II**], the film growth temperatures are here given by the substrate temperature T_s. When spraying alcoholic solutions, the T_{sn} of 250 and 330 °C correspond to T_s of 210 and 280 °C, respectively. The films from aqueous spray solutions were deposited at various growth temperatures T_s = 205 up to 410 °C. The In_2S_3 films from alcoholic spray solutions were grown at 210 and 280 °C. We were unable to characterize the films deposited from alcoholic spray solutions at T_s above 280 °C due to drastic decrease in the film thicknesses.

3.1.1 Structure and phase composition of sprayed In_2S_3 thin films

XRD study was used to characterize the phase composition, preferred orientation of crystallites, lattice parameters as well as the crystallite sizes of the In_2S_3 films deposited by CSP. Figures 3.1 and 3.2 present XRD patterns of the films deposited from aqueous and alcoholic spray solutions with the In:S molar ratios of 1:3 and 1:6 at different growth temperatures.Thin films deposited from aqueous (with T_s = 205 – 365 °C) and alcoholic (with T_s = 210 and 280 °C) spray solutions with the In:S molar ratios of 1:3 and 1:6, exhibit diffraction peaks belonging to the tetragonal β-In_2S_3 phase (JCPDS Card No. 01-074-7284) [24]. No other crystalline phases were detected.

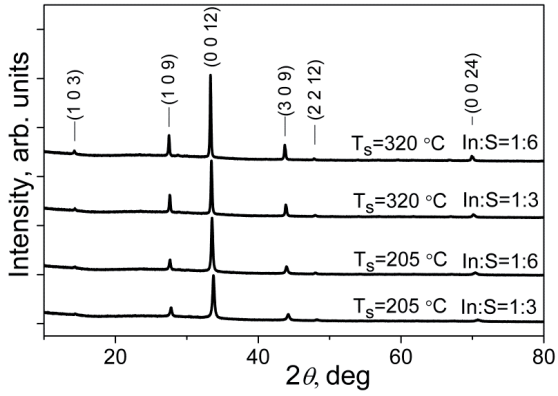

Fig. 3.1. XRD patterns of In_2S_3 films grown at T_s of 205 and 320 °C by using the In:S molar ratios of 1:3 and 1:6 in the aqueous spray solution.

Table 3.1. Lattice parameters (a, b and c) and crystallite size of β-In_2S_3, film thicknesses and optical bandgap (E_g) values of the films deposited at different growth temperatures using precursor molar ratios of In:S = 1:3 and 1:6 in aqueous spray solutions. Determination of E_g for indirect and direct transitions is shown in Fig. 3.7.

	T_s, °C	a=b, Å	c, Å	Crystallite size, nm	Film thickness, nm
In:S =1:3	205	7.553	31.98	35	550
	275	7.600	32.20	63	340
	320	7.608	32.21	64	330
In : S=1:6	205	7.585	32.08	41	450
	275	7.607	32.26	59	350
	320	7.614	32.24	76	380

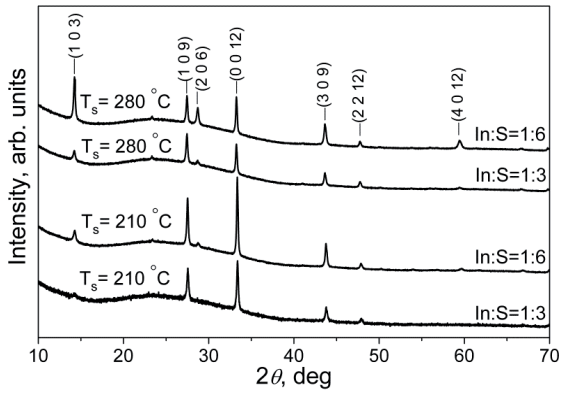

Fig. 3.2. XRD patterns of In_2S_3 films grown at T_s of 210 and 280 °C at the precursors molar ratios of In:S = 1:3 and 1:6 in the ethanol-water solvent spray solutions.

The ratio of the intensities of the (0 0 12) and (1 0 9) diffraction peaks ($I_{(0\ 0\ 12)}/I_{(1\ 0\ 9)}$) is ca. 5 for the films deposited from aqueous solutions (Fig. 3.1). For the powder reference, the $I_{(0\ 0\ 12)}/I_{(1\ 0\ 9)}$ = 0.4 (JCPDS Card No. 01-074-7284) [24]. Thus, β-In_2S_3 films with preferential orientation along the (0 0 12) plane parallel to the substrate were deposited at temperatures up to T_s = 320 °C, using the In:S molar ratios of 1:3 and 1:6 in aqueous spray solutions. For the films deposited at T_s=365 °C using an aqueous spray solution, and at T_s=210 and 280 °C using an alcoholic spay solution, the (1 0 3) and (2 0 6) reflections became more apparent and the relative intensity of the (0 0 12) peak decreased (Figs. 3.2 and 3.3 (a, b)).

John et al. reported that the sprayed β-In_2S_3 films deposited at 300 °C using aqueous spray solutions with the In:S molar ratios of 2:3, 1:2, 2:5, 1:3, 2:7 and 1:4 show the preferred orientation of the crystallites along the (2 2 0) plane [(JCPDS card 25-390) in 47]. According to the β-In_2S_3 powder reference file (JCPDS Card No. 00-025-0390) [24], the reflection at 2θ = 33.45° obviously belongs to the (0 0 12) plane of the β-In_2S_3 film. Moreover, the reflection of the (2 2 0) plane is not given in the β-In_2S_3 powder reference file (JCPDS Card No. 00-025-0390) [24]. Presumably, John et al. made a mistake assigning the reflections in the XRD pattern. Probably a β-In_2S_3 film in [47] had the preferential orientation of the crystallites along the (0 0 12) plane parallel to the substrate.

The lattice constants of the In_2S_3 films increased slightly by increasing the growth temperature from 205 to 320 °C (Table 3.1) and approached the values characteristic of the β-In_2S_3 powder reference (a=b=7.617 Å, c=32.33 Å) (JCPDS Card No. 01-074-7284) [24]. The lattice constants of the In_2S_3 film grown by using the aqueous spray solution with the In:S molar ratio of 1:6 were higher than those obtained from the In:S=1:3 solution at similar temperatures (Table 3.1).

For the films deposited from an aqueous solution with In:S molar ratios of 1:3 and 1:6, the increase in the crystallite size was observed with increasing the growth temperature from 205 up to 320 °C (Table 3.1). The increase of the crystallite size with an increase in the growth temperature has also been observed for the sprayed In_2S_3 films in the literature [47, 48].

The effect of the In:S molar ratio on the size of crystallites becomes obvious using the higher film growth temperatures of about 365 °C. The crystallite size of the films deposited with the In:S molar ratio of 1:6 was ca. 70 nm, while the films deposited with the In:S = 1:3 at similar temperature has the crystallite size of ca. 31 nm. According to the XPS analysis (see Section 3.1.3), the higher amount of oxygen in the films was detected deposited from an aqueous spray solution with the In:S = 1:3 at T_s = 365 °C. It refers to the presence of a secondary phase, which presumably retards the crystallite growth.

The effect of the In:S molar ratio in the aqueous spray solution on the phase composition became notable in the films grown at T_s = 410 °C. The XRD pattern of the film deposited with the In:S molar ratio of 1:3 (see Fig 3.3, pattern c), shows mainly the presence of the crystalline In_2O_3 phase (JCPDS Card No. 01-071-2195) [24] and weak reflections of (1 0 3) and (1 0 9) planes belonging to the crystalline In_2S_3 phase (JCPDS Card No. 01-074-7284) [24]. However, the films deposited with the In:S molar ratio of 1:6 at a similar temperature (T_s = 410 °C) resulted in the mixture of crystalline In_2S_3 and In_2O_3 phases (Fig. 3.3 pattern d). Thus, the

formation of the crystalline oxide phase was favored in the case of the film grown with the In:S molar ratio of 1:3 in the precursor solution. To study the cause of metal oxide formation, the In_2S_3 film grown from the aqueous solution at T_s = 230 °C, with the In:S molar ratio of 1:3 was annealed for 30 min at 450 °C in air. According to XRD analysis (Fig. 3.4), the annealed film is composed of β-In_2S_3 (JCPDS Card No. 01-074-7284) [24]. Thus, the formation of the In_2O_3 phase in the films deposited at T_s = 410 °C was not because of the oxidation of the In_2S_3 phase at this temperature.

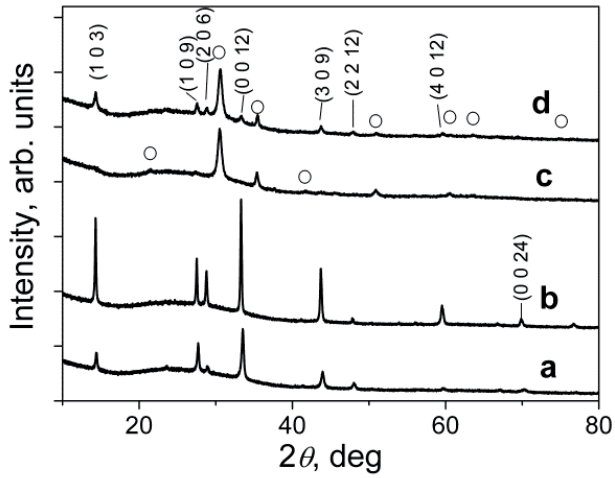

Fig. 3.3. XRD patterns of In_2S_3 films deposited by using aqueous solutions with In:S molar ratios of 1:3 (a) and 1:6 (b) at T_s = 365 °C; and with In:S = 1:3 (c) and 1:6 (d) at T_s = 410 °C. The peaks identified belong to the In_2S_3 phase (JCPDS Card No. 01-074-7284) [24]. The peaks marked with "○" belong to the In_2O_3 phase (JCPDS Card No. 01-071-2195) [24].

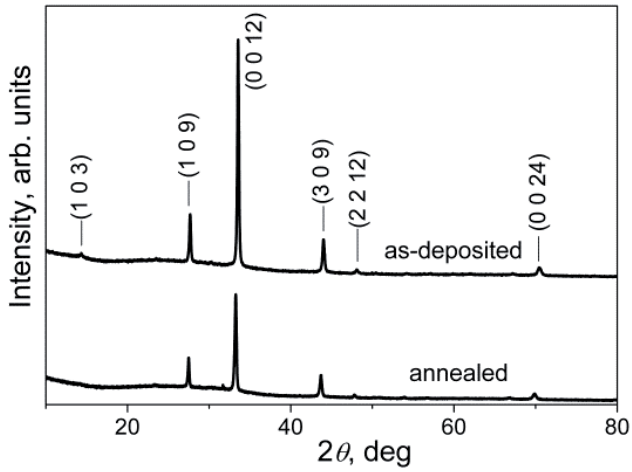

Fig. 3.4. XRD patterns of In_2S_3 films deposited by spray of the aqueous solution with the In:S molar ratio of 1:3 at T_s = 230 °C, and after annealing the film at 450 °C in air.

To summarize, irrespective of the In:S molar ratio in the spray solution the sprayed indium sulfide films grown at temperatures up to 365 °C (using aqueous spray solution) and up to 280 °C (using alcoholic spay solution) are composed of crystalline β-In_2S_3 phase (Figs. 3.1, 3.2, 3.3 patterns a, b). The films grown at T_s = 410 °C from aqueous spray solution with the In:S molar ratio of 1:3 primarily consisted of crystalline In_2O_3 phase. However, the films deposited from an aqueous solution with the molar ratio of In:S = 1:6 at T_s = 410 °C contained a mixture of In_2S_3 and In_2O_3 phases (Fig. 3.3 patterns c, d). We found that In_2O_3 phase in the sprayed indium sulfide film deposited at temperatures around 400 °C is not due to the oxidation of In_2S_3.

3.1.2 Morphology and optical properties of sprayed In_2S_3 thin films

SEM study

SEM images were used to study the influence of the different deposition parameters on the film morphology and thicknesses. According to SEM images, the In_2S_3 films grown either from aqueous or alcoholic spray solutions with the In:S molar ratio of 1:3 and 1:6, exhibit uniform coverage of the substrate with no cracks or pinholes (Fig. 3.5). The molar ratio of the In:S in an aqueous and alcoholic spray solutions was found to have an insignificant effect on the film thickness and grain size of the films grown at similar temperatures.

The In_2S_3 films grown by spray of aqueous spray solutions at T_s = 205 °C are composed of grains with the size of ca. 150 – 300 nm (Fig. 3.5 a). These grains seem to be aggregates of smaller crystallites sized of ca. 35 nm (Table 3.1). According to XPS studies, the films grown at 205 °C contained chlorine residues (see Section 3.1.3). Thus, the formation of aggregates could be due to the sintering effect of chlorine containing compounds on the surface of the grains (likely residues of $InCl_3$). In the films deposited at T_s = 275 °C with an aqueous solvent (Fig.3.5 b) and at T_s = 210 °C with an alcoholic spray solution (Fig.3.5 c) grain sizes of ca. 40 – 150 nm were observed, indicating that some of the crystallites aggregate to form larger grains and other crystallites do not.

However, the SEM study shows that the film thickness and surface morphology strongly depends on the solvent. In_2S_3 films deposited from an aqueous spray solution at T_s = 205 °C show a thickness of ca. 500 nm. The films grown from alcoholic solutions at T_s = 210 °C show a thickness of ca. 150 nm and ca. 130 nm using ethanol-water and isopropanol-water solutions, respectively (Fig. 3.5).

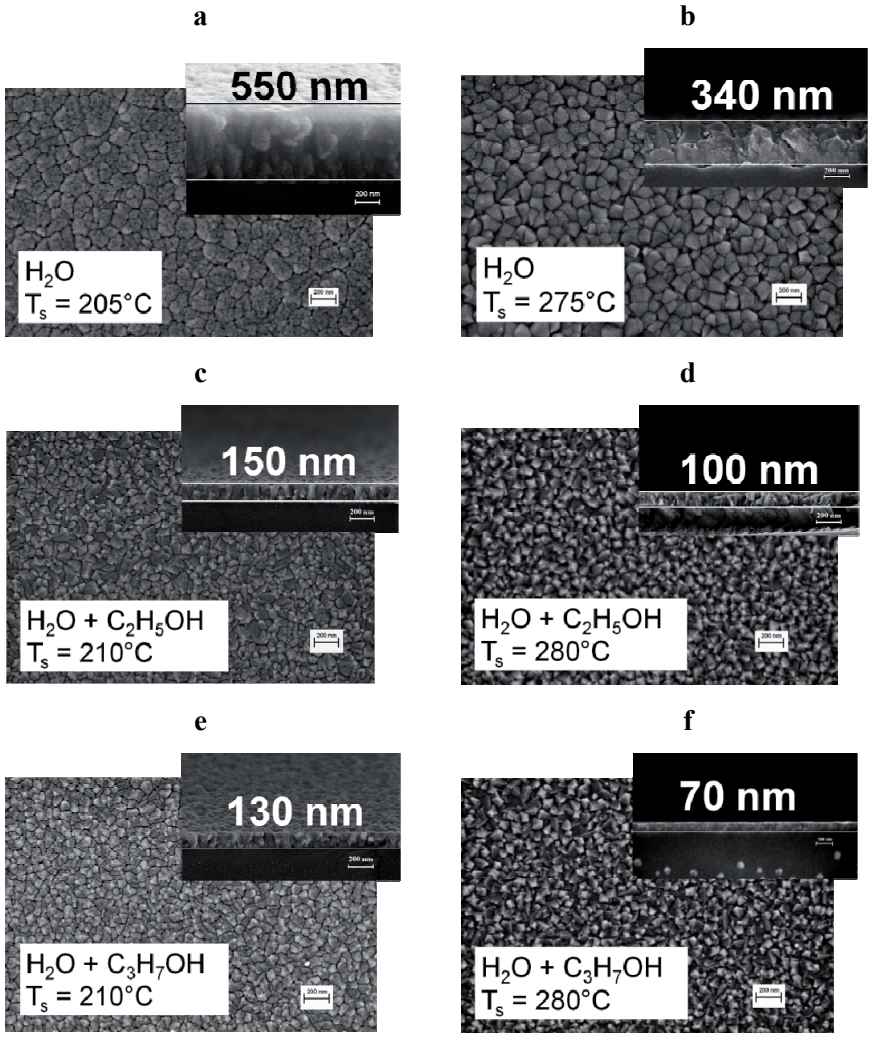

Fig. 3.5. SEM micrographs of the films deposited from the spray solutions with the $InCl_3$:$SC(NH_2)_2$ molar ratio of 1:3 at different temperatures, using different solvents.

In_2S_3 films deposited at 210 and 280 °C by using alcoholic spray solutions were more compact and homogeneous compared to the films grown from aqueous solutions at similar growth temperatures (Fig. 3.5). Much lower thickness of the films sprayed from the alcoholic solution could be explained by the convection induced repelling of smaller droplets from the reaction zone. The smaller droplets are formed by spraying alcoholic solutions instead of aqueous ones [111], since alcohols have lower surface tension than water [76]. For example, the used ethanol-water mixture (1:1 by volume) has the surface tension of ca. 29 mN/m, which is noticeably lower than the surface tension of water of ca. 72 mN/m [138].

To summarize, irrespective of the used solvent the film thicknesses decrease with an increase in the film growth temperature (Fig. 3.5). The spray of alcoholic solutions instead of aqueous solutions at similar growth temperatures resulted in more compact but thinner films with smaller grain sizes (Fig 3.5).

Optical properties

The UV-VIS study was performed to characterize the total optical transmittance and to determine the optical bandgap of the In_2S_3 thin films deposited by varying different deposition parameters. The In_2S_3 films deposited from aqueous spray solutions with the In:S molar ratio of 1:6 at T_s= 205 – 365 °C show the total optical transmittance around 70 % in the visible and near-infrared spectral region (Fig. 3.6), the total optical transparency decreased slightly with increasing the growth temperature from 205 to 365°C. At the same time the number of interference fringes decreases indicating to the decrease in the film thickness. The decrease in the film thickness increasing the film growth temperature (from 205 °C to 320 °C) is confirmed by the SEM cross-sectional images (Table 3.1, Fig. 3.5). A decrease in the film thickness with an increasing growth temperature is a phenomenon characteristic of spray-deposited films [11]. In_2S_3 films deposited from the aqueous spray solution with the In:S molar ratio of 1:3 showed similar behaviour.

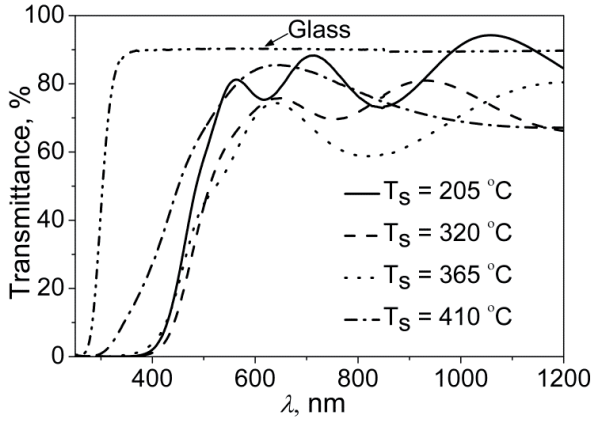

Fig. 3.6. Total optical transmission spectra of In_2S_3 films grown from aqueous spray solutions at different growth temperatures using the precursor solution with the In:S molar ratio of 1:6. Transmission spectrum of a bare glass substrate is presented for comparison.

The optical bandgap (E_g) values were determined from the well-known equation (Eq. 3.1) for the allowed transitions:

$$\alpha h\nu = A(h\nu - E_g)^{1/n} \quad , \qquad (3.1)$$

where α is the absorption coefficient calculated from the optical spectra, A is a constant, h is the Planck constant, E_g is the bandgap energy, $h\nu$ is the incident

photon energy and 1/n is the exponent that depends on the nature of the optical transition (n = 0.5 and 2 for direct and indirect transition, respectively).

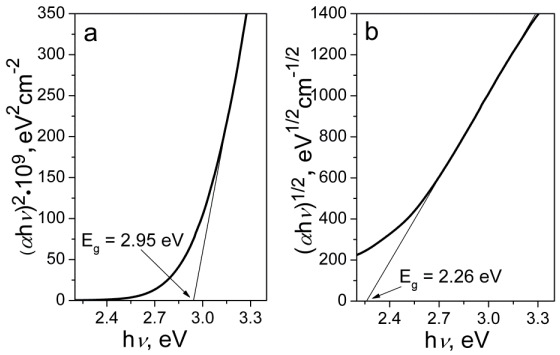

Fig. 3.7. Graphical determination of direct (a) and indirect (b) optical bandgaps of In_2S_3 films deposited from In:S =1:6 aqueous spray solution at T_s = 230 °C.

The optical bandgap values of In_2S_3 films were calculated from the total optical transmittance, assuming the indirect and direct transition type for the films deposited from aqueous and alcoholic spray solutions (Fig. 3.7, Table 3.2).

Table 3.2. Optical bandgap (E_g) values of films deposited at different growth temperatures using precursor molar ratios of In:S = 1:3 and 1:6 in aqueous and alcoholic spray solutions. Determination of the E_g for indirect and direct transitions is shown in Fig. 3.7.

	Solvent	T_s, °C	$E_{g\ indirect}$, eV	$E_{g\ direct}$, eV
In:S=1:3	H_2O	205	2.30	2.94
		275	2.21	2.90
		320	2.17	2.92
		365	2.08	3.14
		410	-	3.65
	H_2O:C_2H_5OH	210	2.00	2.97
		280	2.00	2.97
	H_2O:C_3H_7OH	210	2.00	2.88
		280	2.00	2.92
In:S=1:6	H_2O	205	2.28	2.96
		275	2.19	2.93
		320	2.15	2.92
		365	2.14	2.91
		410	-	3.64
	H_2O:C_2H_5OH	210	2.00	2.91
		280	2.02	2.97
	H_2O:C_3H_7OH	210	2.00	2.97
		280	2.03	2.96

The E_g values of the In_2S_3 films deposited from aqueous spray solutions at temperatures $T_s < 365$ were in the range of 2.15 – 2.30 eV (indirect transitions) and around 2.90 eV (direct transitions) irrespective of the In:S in the aqueous solution (see Table 3.2). These values are close to those reported earlier for the CSP deposited [139] as well as for the spray-ILGAR [42] and CBD deposited [40] indium sulfide films.

The effect of the In:S molar ratio in the aqueous spray solution became apparent when the films were deposited at $T_s \geq 365$ °C (Table 3.2). The direct bandgap value increases up to 3.14 eV for the films deposited at 365°C spraying an aqueous solution with the In:S = 1:3. No increase in the direct bandgap value was observed for the film grown with the In:S = 1:6 in the spray solution (Table 3.2). The increase in E_g values may be due to the higher oxygen content in the films deposited from the aqueous spray solution with the In:S molar ratio of 1:3, as was confirmed by XPS (see Section 3.1.3). Irrespective of the In:S molar ratio in the spray solution, the direct E_g values for the films deposited at 410 °C were ca. 3.65 eV (Table 3.2), corresponding to those reported for the In_2O_3 [140]. The presence of crystalline In_2O_3 phase in the films grown at T_s = 410°C was confirmed by XRD (see Section 3.1.1 and Fig. 3.3 patters c, d).

For the In_2S_3 films deposited from alcoholic spray solutions with the In:S molar ratios of 1:3 and 1:6 at T_s = 210 and 280 °C, the indirect E_g values were ca. 2.00 eV and the direct E_g values were in the range of 2.88 – 2.97 eV (Table 3.2). The indirect E_g value is slightly lower than 2.2 eV and 2.2 – 2.4 eV reported by M. Calixto-Rodriguez et al. [48] and Kim et al. [48], respectively, for the In_2S_3 films deposited by spray of alcoholic solutions. However, the indirect E_g value of 2.0 eV is close to that reported for ALD-deposited In_2S_3 films [56].

To summarize, it was found that In_2S_3 films grown at T_s below 365 °C exhibited transparency over 70% in the visible spectral region and E_g of 2.15 – 2.30 eV (indirect transitions) and around 2.90 eV (direct transitions), irrespective of the In:S molar ratio in the aqueous solution. The effect of the In:S molar ratio in the aqueous spray solution became apparent for the films deposited at T_s = 365 °C. A higher E_g value was determined for the film sprayed from the aqueous solution with In:S = 1:3, compared to the E_g value for the film sprayed with In:S = 1:6 at T_s = 365 °C. The films deposited from aqueous spray solutions with In:S molar ratios of 1:3 and 1:6 at 410 °C show the direct E_g value indicating to the occurrence of In_2O_3.

3.1.3 Elemental composition of sprayed In_2S_3 thin films

The XPS and EDX were used to study the influence of the different deposition parameters on the chemical composition of the sprayed In_2S_3 films. The core level peaks of $In3d_{5/2}$, S2p and O1s from the un-cleaned and Ar^+ ion sputtered surfaces were detected from the XPS spectra of all studied films (Figs. 3.8, 3.9). No shift in the $In3d_{5/2}$, S2p (Fig. 3.8) and Cl2p (spectrum is not presented) peak positions was observed before and after Ar^+ ion sputtering. However, the O1s peak from the un-cleaned surfaces for all studied films could be separated into three sub-bands positioned at BE = 530.0, 531.3 and 532.4 eV (Fig. 3.8). The O1s peaks at 531.3 and 532.4 eV are characteristic of C = O, OH^- and adsorbed water, respectively;

therefore both peaks can be attributed to the surface contamination [141, 142]. The peak with the BE of 530.0 eV is characteristic of oxygen bonded to metal (Me – O) [102]. The peak positions of the $In3d_{5/2}$, S2p and Cl2p core level peaks at BE = 444.7 eV, 161.6 eV (Fig. 3.8), respectively are similar to those reported for spray-deposited β-In_2S_3 [103].

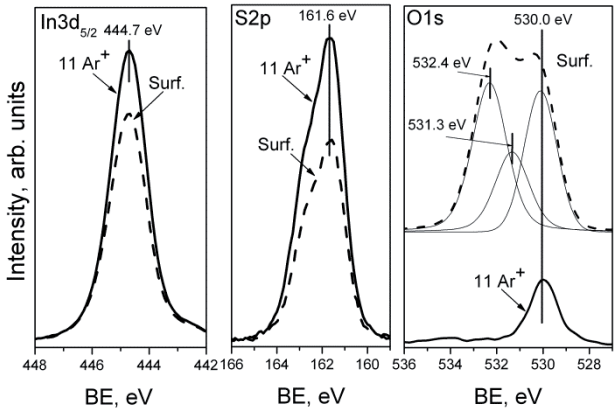

Fig. 3.8. $In3d_{5/2}$, S2p and O1s core level spectra recorded from the surface of the sprayed film and from the surface after 11 Ar^+ ion sputtering cycles. In_2S_3 films were deposited at 365 °C using the precursor molar ratio of In:S = 1:3 in the aqueous spray solution.

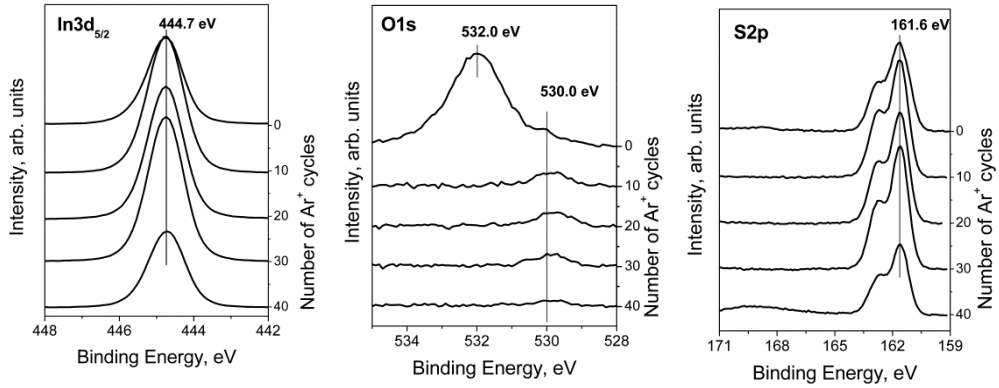

Fig. 3.9. $In3d_{5/2}$, S2p and O1s core levels spectra of In_2S_3 film deposited at T_s = 275 °C (In:S =1:3 in the aqueous spray solution) taken from the film surface and after different Ar^+ sputtering cycles.

The peak intensity of the oxygen bonded to metal at BE = 530.0 eV was higher for the film deposited with the In:S molar ratio of 1:3 in the aqueous solution at 365 °C (Fig. 3.8), compared to the film grown at 275 °C (Fig. 3.9) using an aqueous solution. According to the XPS depth profiling (Fig. 3.9), all of the studied In_2S_3 films grown at the temperature region of 205 – 365 °C with the In:S molar ratio of

1:3 and 1:6 in the solution showed a uniform distribution of the elements through film thickness.

The relative values of the elemental compositions in atomic percentages were calculated from the integrated areas of $In3d_{5/2}$, S2p, O1s and Cl2p core level peaks. Table 3.3 summarizes the relative composition of the films depending on the growth temperature and the molar ratio of In:S (1:3 vs. 1:6) in the aqueous and alcoholic spray solution.

Table 3.3. The relative values for the elemental composition (in at.%) of In_2S_3 films calculated from the XPS spectra. The films were deposited using In:S molar ratios of 1:3 and 1:6 in aqueous or alcoholic spray solutions at different growth temperatures (T_s).

Solvent	T_S, °C	In : S in solut.	Ar^+ etching cycles	In	S	Cl	O, (Me-O)
H_2O	205	1:3	11	43	53	2	2
		1:6	11	44	53	2	1
	275	1:3	10	43	54	1	2
		1:6	10	42	56	1	1
	365	1:3	11	43	52	-	5
		1:6	11	43	56	-	1
H_2O + C_2H_5OH	210	1:3	3	42	55	2	1
		1:6	2	40	57	2	1
	280	1:3	3	42	56	-	2
		1:6	3	43	56	-	1

The presence of oxygen bonded to metal (Me - O, O1s with BE = 530.0 eV) was detected in all sprayed In_2S_3 films, but its amount was significantly lower for the films deposited with the In:S molar ratio of 1:6 (Table 3.3). According to the EDX study the same tendency was observed for the oxygen content in the films, since additional oxygen signals are coming from the glass substrates (Table 3.4).

Table 3.4. Elemental composition (in at.%) of In_2S_3 films according to EDX. The films were deposited at T_s= 365 °C using In:S molar ratios of 1:3 and 1:6 in the aqueous spray solution.

In:S in solut.	In	S	Cl	O	Si	Na
1 : 3	34	43	1	15	5	2
1 : 6	33	45	<1	12	7	2

The Cl2p peak was detected in the films deposited from the aqueous spray solutions at T_s = 205 and 275 °C and in the films from alcoholic spray solutions at T_s = 210 °C, irrespective of the In:S molar ratio in the spray solution (Table 3.3).

Chlorine contamination originates from the $InCl_3$ precursor and decreases with the increase of the growth temperature. According to XPS and EDX, no chlorine was detected or its concentration was relatively low in the films deposited from aqueous spray solutions at T_s = 365 °C (Tables 3.3, 3.4) and from alcoholic solutions at T_s = 280 °C (Table 3.3). The decrease in the chlorine content with an increasing growth temperature has been generally observed for spray deposited films [2].

To summarize, similar results were received from XPS and EDX studies. Both of the methods show that the oxygen contamination in the In_2S_3 films can be minimized by using the spray solution with the In:S molar ratio of 1:6. According to XPS, all sprayed In_2S_3 films show a uniform distribution of the elements throughout the film.

3.1.4 Summary of the deposition of sprayed In_2S_3 thin films

It is shown that β-In_2S_3 thin films could be successfully deposited by the low-cost pneumatic spray pyrolysis method in air, using aqueous or alcoholic spray solutions containing $InCl_3$ and $SC(NH_2)_2$. Irrespective of the In:S molar ratio in aqueous spray solutions the films grown at temperatures up to T_s = 365 °C are orientated along the (0 0 12) plane parallel to the substrate, with E_g of 2.15 – 2.30 eV (indirect transitions) and around 2.90 eV (direct transitions). β-In_2S_3 films deposited at T_s = 210 and 280 °C using alcoholic solutions with the In:S molar ratios of 1:3 and 1:6, with E_g of ca. 2.00 eV (indirect transitions) and with E_g of 2.88 – 2.97 eV (direct transitions). Spraying of alcoholic solutions leads to thinner but more compact films.

According to the study, when films were deposited at $T_s \geq 365$ °C**,** the content of oxygen in sprayed In_2S_3 films was to a great extent controlled by the In:S molar ratio in the aqueous spray solution. The film grown at 410 °C from the aqueous spray solution with In:S = 1:3 was composed mainly from the crystalline In_2O_3 phase, while the film deposited from In:S = 1:6 in spray solution was composed from the mixture of In_2S_3 and In_2O_3 crystalline phases by XRD analysis.

In order to understand the effect of the sulfur source content in the spray solution on the In_2S_3 film properties and the possible origin of the oxygen content in the films it is necessary to study the formation of the In_2S_3 in CSP process. In other words, knowledge of formation chemistry allows us to determine the optimal solution composition and thermal conditions of CSP and thereby control properties of the sprayed In_2S_3 thin films. This is important because we plan to expand the studies further - to spray deposit In_2S_3 films doped with Ti, to be used as an absorber material in two-photon absorption processes based solar cells.

3.2 Formation of In_2S_3 in spray pyrolysis process

In order to study the formation of In_2S_3 in the spray pyrolysis process, aqueous solutions containing $InCl_3$ and $SC(NH_2)_2$ at the molar ratio of 1:3 (**1**) and 1:6 (**2**) were prepared, then the solvent was let to evaporate, and the obtained powder samples were further used for structural and thermal decomposition studies (see

more details in Section 2.2, Table 2.2). The results are published in papers [**III**] and [**IV**].

3.2.1 Characterization of the precursors for indium sulfide thin films by CSP

Characterization of samples **1** and **2** as precursors for thermal analysis by FTIR spectroscopy, XRD and elemental analysis is presented in this subsection. The results are published in [**III**, **IV**].

Interaction of $InCl_3$ and $SC(NH_2)_2$ in an aqueous solution

Figure 3.10 shows a comparison of the FTIR spectra of the dried samples **1**, **2** and $SC(NH_2)_2$ (thiourea). The vibrations that peaked at 1473 and 1085 cm^{-1} in the spectrum of thiourea ligand are characteristic of the CN group stretching vibrations, ν (CN) [118]. In the spectrum of **1** and **2**, the ν(CN) vibrations were shifted towards higher frequencies of 1504 and 1102 cm^{-1}, respectively (Fig. 3.10). The increased wavenumbers of the CN group vibrations in **1** and **2** indicate the strengthening of the bond between carbon and nitrogen atoms [118, 143, 144] (Fig. 3.11). IR spectrum of the free thiourea ligand exhibits strong and sharp vibrations at 730 and 630 cm^{-1} characteristic of CS group stretching vibrations, ν(CS) [118, 124, 125]. The shift of ν(CS) vibrations towards lower wavenumber of 700 cm^{-1} in **1** and **2**, compared to that in thiourea, is due to the reduced double bond character between carbon and sulfur atoms [124, 125, 143] (Fig. 3.11) The observed shifts of ν(CS) and ν(CN) vibrations indicate the formation of the complex compound as was also observed in the case of the Cd, Cu and Zn chloride complexes with thiourea [118, 125, 126]. For **2** additional peaks at 1473, 1085, 730 and 630 cm^{-1} can be observed, which are characteristic of ν(CN) and ν(CS) in thiourea (Fig. 3.10).

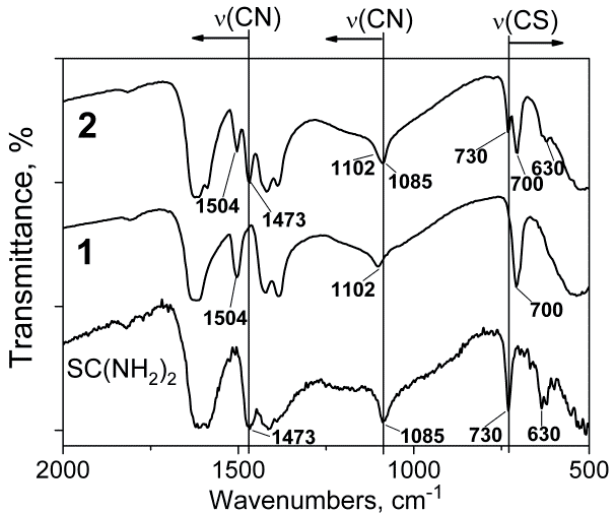

Fig. 3.10. FTIR spectra of dried samples **1**, **2** and $SC(NH_2)_2$ recorded at room temperature.

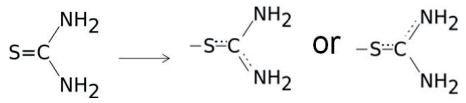

Fig. 3.11. Scheme of the bond change character in $SC(NH_2)_2$.

The XRD pattern of **1** remained unidentified, but in pattern **2**, besides the unidentified phase the peaks characteristic of $SC(NH_2)_2$ phase (JCPDS Card No. 00-031-1934) were detected [24]. No crystalline $InCl_3$ phase was detected in **1** and **2** (not shown).

According to elemental analysis, the elemental composition of **1** (found, in mass%) is: S 20.1%, Cl 23.4%, C 7.7%, N 18.8% and H 2.3%. The composition of **2** (found, in mass%) is: S 27.4%, C 10.3%, N 24.5%, H 3.5% [**III**]. The elemental composition of **1** is close to that calculated for a compound with a hypothetical formula $InCl_3 \cdot 3(SC(NH_2)_2)$: In 25.5%, Cl 23.7%, S 21.4%, C 8.0%, N 18.7%, H 2.7%. The composition of **2** is close to that calculated for a mixture of $InCl_3 \cdot 3(SC(NH_2)_2)$ + $3(SC(NH_2)_2)$: In 17.0%, Cl 15.7%, S 28.4%, C 10.6%, N 24.8%, H 3.5%.

According to the chemical analysis with the results from FTIR and XRD, the sample **1** is a complex compound where all thiourea is coordinated to the indium atom through the sulfur atom and can be expressed by a hypothetical formula $InCl_3 \cdot 3(SC(NH_2)_2)$ (named below as $In(tu)_3Cl_3$) [**III, IV**]. The sample **2** is composed from a thiourea complex compound and free thiourea with a hypothetical formula $InCl_3 \cdot 3(SC(NH_2)_2)$ + $3(SC(NH_2)_2)$ (named below as $In(tu)_3Cl_3$ + 3tu) [**III**].

Crystal structure of $In(tu)_3Cl_3$

According to the single crystal XRD analysis made by Dr. Petra Bombicz (Institute of Structural Chemistry, Hungarian Academy of Sciences, Hungary) [**IV**], the **1** ($In(tu)_3Cl_3$) is: *mer*-trichlorotris(thiourea)- with the molecular formula - $C_3H_{12}Cl_3InN_6S_3$, Fwt.: 449.55, triclinic crystal system, space group *P*-1, a = 8.4842(2) Å, b = 10.5174(2) Å, c = 13.1767(2) Å, α = 111.1870(10)°, β = 98.0870(10)°, γ = 97.889(2)°, V = 1062.63(4) $Å^3$, Z = 3, Z' = 1.5, $F(000)$ = 220, Dx = 2.098 Mg/m^3, μ = 22.570 mm^{-1} [**IV**]. The structure of $In(tu)_3Cl_3$ (**1**) is presented in Fig. 3.12. Although the structure of $In(tu)_3Cl_3$ obtained by using aqueous solutions containing $InCl_3$ and thiourea with the molar ratio of $SC(NH_2)_2$:$InCl_3$=K, where K=3, was reported in 1992 [136], the crystal structure of $In(tu)_3Cl_3$ is improved and refined in the paper published in 2011 [**IV**].

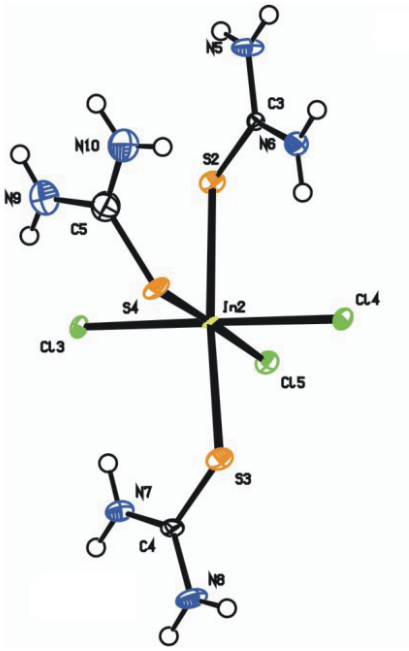

Fig. 3.12. The crystal structure of the $In(tu)_3Cl_3$ (**1**).

3.2.2 Thermal analysis of precursors for In_2S_3 films

The thermal decomposition process of the complex $In(tu)_3Cl_3$ (**1**) and of that with addition of free, noncomplexed thiourea ($In(tu)_3Cl_3$ + 3tu) (**2**) were characterized by simultaneous TG/DTA/EGA-FTIR measurements in 80%Ar + 20%O_2 (air) atmosphere using the heating rate of 10 °C min^{-1} [**III**, **IV**]. For **1** the thermal analysis was also conducted in both an inert and air atmospheres by simultaneous TG/DTA/EGA-MS techniques using the heating rate of 10 °C min^{-1} [**IV**]. XRD and FTIR were used *ex situ* to identify the solid intermediates and the final products of their thermal decomposition [**III, IV**].

The thermal decomposition of **1** in nitrogen atmosphere consisted from three mass loss steps in the temperature region of 205 – 750 °C (Table 3.5). The first mass loss step occurs in the temperature range of 205 – 275 °C with a mass loss of ca. 34%. In the first mass loss step, four sequential endothermic processes with maxima at 210, 215, 230 and 255 °C (Fig. 3.13 a, Table 3.5) occurred. The second decomposition step in the temperature range of 275 – 405 °C was an endothermic process with the DTA maximum at 320 °C (Fig. 3.13 a, Table 3.5). The mass loss in the second step was 13.2%. The third decomposition step contained an endothermic peak with a maximum at 610 °C in the temperature region of 405 – 750 °C with the mass loss of 29.1% (Fig. 3.13 a, Table 3.5). The total mass loss for **1** in nitrogen atmosphere was 76.1% (Table 3.5).

Table 3.5. Decomposition steps, mass losses and temperatures of DTA peaks of dried powders of **1** and **2**, recorded using the heating rate of 10°C min^{-1} in air and nitrogen atmospheres

Sample	Atmosphere	Step	TG temp. range, °C	DTA peak (+/-), °C	Mass loss, %
1	N_2	1	205-275	210 (-) 215 (-) 230 (-) 255 (-)	33.9
		2	275-405	320 (-)	13.2
		3	405-750	610 (-)	29.1
				Total mass loss	76.1
1	air	1	205-300	210 (-) 220 (-) 230 (+) 270 (-)	34.8
		2	300-520	355 (-)	26.4
		3	520-680	580 (+) 610 (+) 650 (+)	24.6
		4	680-730	710 (+)	3.3
				Total mass loss	89.1
2	air	1	180-300	160 (-) 205 (-) 210 (-) 215 (+) 220 (-) 240 (+) 270 (+)	50.7
		2	300-400	335 (-)	9.6
		3	400-680	450 (-)	10.2
		4	680-790	715 (+) 760 (+) 770 (+)	8.0
				Total mass loss	78.5

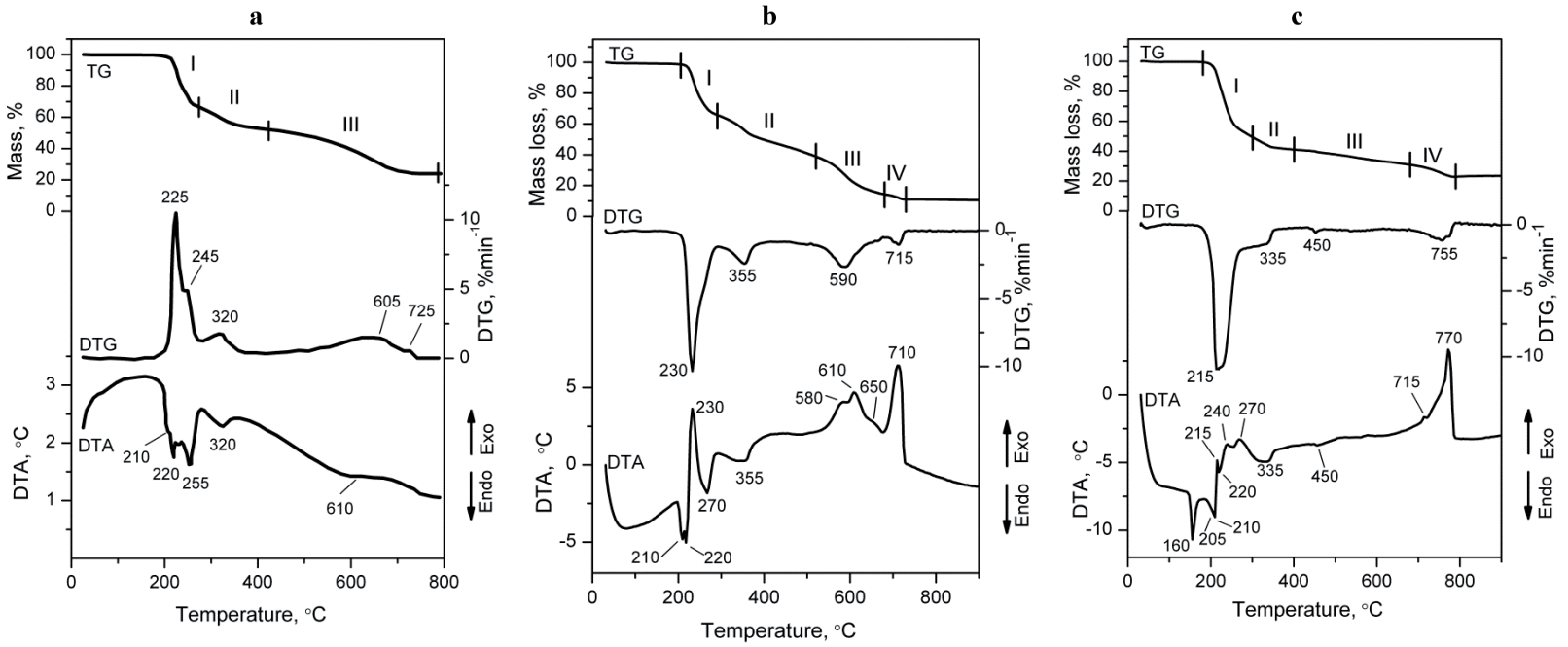

Fig. 3.13. Simultaneous TG, DTG and DTA curves of **1** (a) recorded in N_2 flow 130 mL/min, using heating rate of 10 °C min^{-1}; **1** (b) and **2** (c) recorded in 80%Ar + 20%O_2 flow 60 mL/min, using heating rate of 10 °C min^{-1}. Initial sample mass for **1** (a) - 8.7 mg in N_2 atmosphere; **1** (b) - 7.8 mg and for **2** (c) - 7.4 mg in air.

According to XRD, the final solid decomposition product of **1** in nitrogen consisted from In_2S_3 (JCPDS Card No. 01-074- 7284) [24] and In_2O_3 (JCPDS Card No. 01-071-2194) [24] in amount of 92% and 8%, respectively. Although during the thermal decomposition of **1** in nitrogen atmosphere no exothermic effects were observed (Fig. 3.13 a, Table 3.5), the presence of traces of In_2O_3 in the final product refers to the presence of oxygen somewhere in the system, in gas or in the initial sample. The total mass loss of **1** in nitrogen atmosphere was 76.1 % that is higher than the theoretical value of 64.2%. This result refers to the release of some volatile indium species from the system. Presumably, volatile $InCl_3$ species leave the system, due its relatively high vapor pressure at elevated temperatures (1 atm at around 500 °C [145]). The total mass loss higher than the theoretical one was also observed for the thermal decomposition of the zinc chloride thiourea complex ($Zn(tu)_2Cl_2$) and has been explained by the evaporation of $ZnCl_2$ [117, 119].

According to DTG and TG curves in air, the thermal decomposition of **1** consists from four mass loss steps in the temperature interval of 205 – 730 °C (Fig. 3.13 b, Table 3.5). In the first mass loss step (205 – 300 °C), the thermal degradation of **1** starts with two sequential endothermic effects at 210 °C and 220 °C undergoing a strong exothermic effect with a maximum at 230 °C, and followed by an endothermic effect at 270 °C according to the DTA curve. The first two endothermic effects correspond to the melting and decomposition processes, respectively (Fig. 3.13 b). The exothermic effect at 230 °C is obviously due to the oxidation of the evolved CS_2 vapor [122, 146], as was confirmed by the EGA analysis (see Section 3.2.3). The second decomposition step (300 – 520 °C) is an endothermic process. The third decomposition step (520 – 680 °C) and the fourth step (680 – 730 °C) contain only exothermic effects (Fig. 3.13 b). The total mass loss was 89.1% for **1** in air. According to XRD, the final solid decomposition product of **1** in air was In_2O_3 (JCPDS Card No. 01-073-6440) [24] (Table 3.6). The total mass loss is higher than the calculated 69.1%, indicating that some volatile indium species leave the system.

In conclusion, the thermal decomposition of **1** in nitrogen atmosphere took place in the temperature range of 205 – 750 °C and consisted from three mass loss steps with the total mass loss of 76.1%. The thermal decomposition of **1** in air contained four mass loss steps in the temperature region of 205 – 730 °C with the total mass loss of 89.1%. In both of the atmospheres the total mass loss was higher than the theoretical mass loss, indicating to the release of volatile indium species (e.g. $InCl_3$). The final decomposition product of **1** at 800 °C in nitrogen atmosphere contained small amount of In_2O_3 (8%) phase, referring to the occurrence of the oxygen in the inert atmosphere.

The thermal decomposition study of **2** was conducted only in air and took place in the temperature interval of 180 – 790 °C in four mass loss steps (Fig. 3.13 c). In the first decomposition step (180 – 300 °C) the endothermic effects detected at 160 and 205 °C obviously belong to the melting and the decomposition of thiourea, respectively [146], as in addition to the complex compound $In(tu)_3Cl_3$ (**1**); **2** contains free, noncoordinated thiourea. Endothermic effects at 210 and 220 °C (Fig. 3.13 c), are characteristic of melting and decomposition of the $In(tu)_3Cl_3$, are less pronounced than in the case of **1** (Fig. 3.13 b) due to the exothermic processes

taking place at 215 and 240 °C. The second decomposition step (300 – 400 °C) and the third step (400 – 680 °C) contain only endothermic processes, while the fourth step (680 – 790 °C) is highly exothermic. The final decomposition product of **2** at in air was In_2O_3 (JCPDS Card No. 01-073-6440) [24] by XRD [**III**]. For **2**, the total mass loss of 78.5% is close to the theoretical value of 79.6%, indicating that the excess of thiourea in the precursor hinders the release of volatile indium species from the system.

3.2.3 Study of gaseous and solid products of thermal decomposition of precursors for indium sulfide films

Initially, the thermal analysis of **1** and **2** was made using TG/EGA-FTIR in inert and in air. The unexpected occurrence of gases evolved as a result of the oxidation processes in inert atmosphere (not shown), lead to the study of the thermal decomposition of **1** also by TG/EGA-MS in an inert atmosphere and in air. As a result of TG/EGA-FTIR and TG/EGA-MS studies the evolution of gases was compared and it was found that these two methods complement each other (e.g. the evolution of HNCS is hardly identified by EGA-MS; the evolution of HCl could better be detected by EGA-MS). Although the evolution of gases was similar according to both of the methods, the sequence of gases evolved was more apparent and easier to follow by EGA-FTIR than by EGA-MS. Hence the sequence of the evolved gaseous species is characterized in the order they appeared by EGA-FTIR (Fig. 3.14).

Figure 3.15 depicts the FTIR spectrum of gases evolved from **1** at 240 °C in 80%Ar + 20%O_2 (air). The evolution profiles of gaseous species from **1** and **2** in air as recorded by online TG/EGA-FTIR are compared in Fig. 3.14 [**III**]. Similar gaseous species evolved from **1** and **2** in air in the temperature region around 200 – 350 °C (Fig. 3.14). At higher temperatures, the evolution of CO_2 and H_2NCN with similar evolution profiles with maxima at 580 and 610 °C from **1** has been recorded. In the case of **2** the evolution of these gases was detected with a monotonous increase from 400 °C up to maximum at 770 °C (Fig. 3.14). Figure 3.16 shows the evolution curves of gases from **1** recorded by online TG/EGA-MS in nitrogen and in air [**IV**]. Interestingly, from **1** in the N_2 atmosphere the evolution of gases COS, SO_2, HCN and CO_2 (Fig. 3.14) was detected. The possible reasons for the evolution of these gases will be discussed in following section. In parallel, the results of *ex situ* FTIR (Fig. 3.17) and XRD (Table 3.6) analyses of solid intermediates and final decomposition products are discussed.

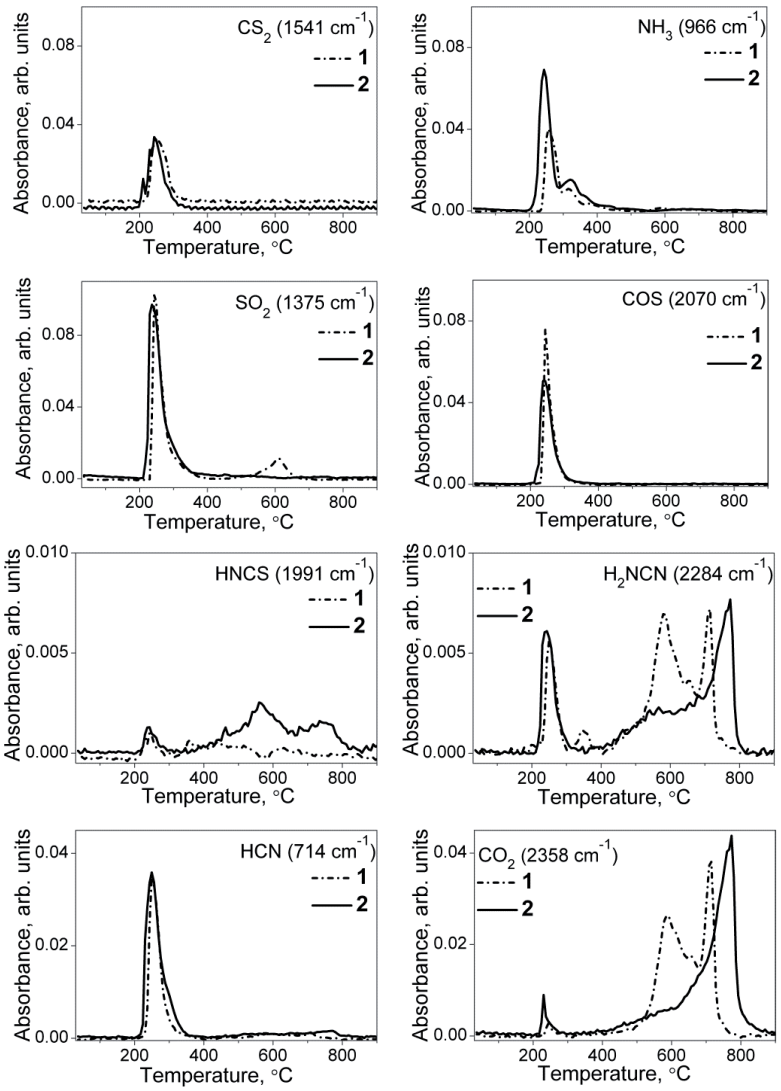

Fig. 3.14. Evolution profiles of gaseous species from **1** and **2** in 80%Ar + 20%O_2, as measured by *in situ* TG/EGA-FTIR system (80%Ar+20%O_2 flow 60 mL/min, heating rate 10 °C/min, initial mass for **1** - 7.8 mg and for **2** - 7.4 mg).

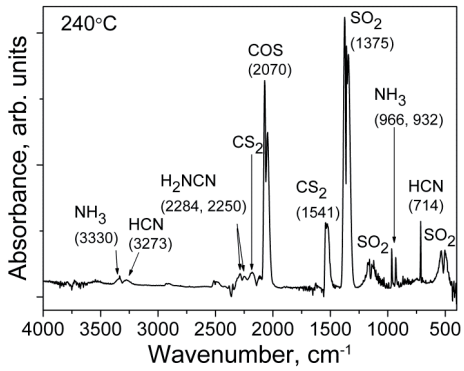

Fig. 3.15. EGA-FTIR spectra of the evolved gases of **1** at 240 °C. Flowing 80%Ar + 20%O_2: 60 mL min^{-1}, heating rate: 10 °C min^{-1}, initial sample mass: 7.8 mg

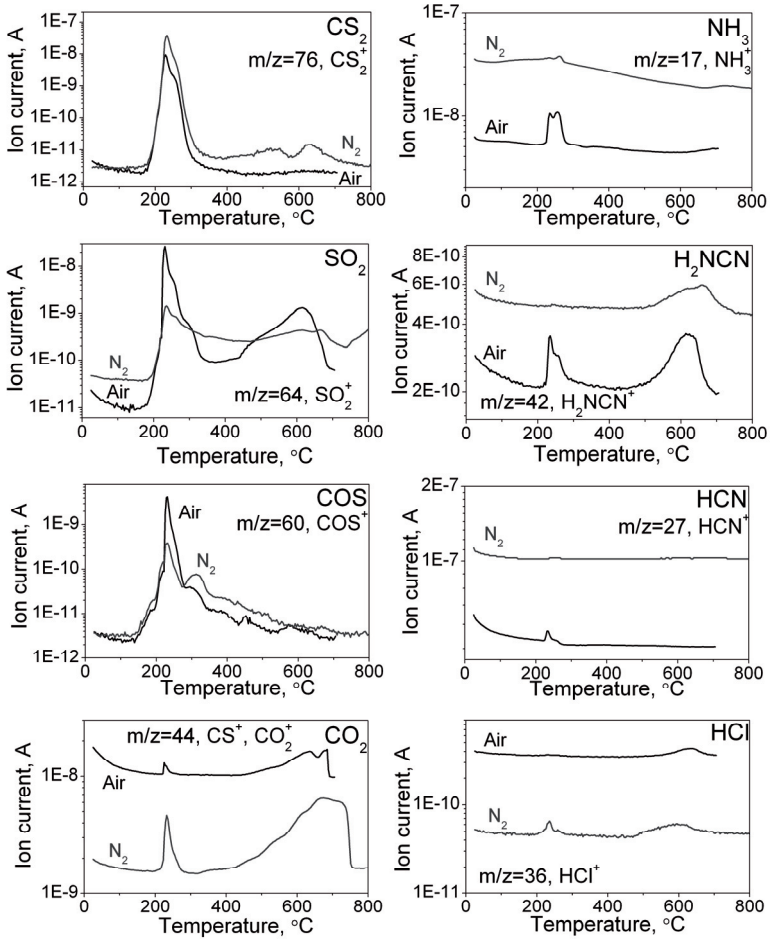

Fig. 3.16. Evolution profiles of various gaseous species represented by their characteristic mass spectroscopic ion fragments, from **1** in nitrogen and in air, as measured by the online coupled TG/DTA/EGA-MS system. N_2 flow 130 mL/min, heating rate 10 °C/min, initial mass 8.71 mg; air flow 130 mL/min, heating rate 10 °C/min, initial mass 9.6 mg.

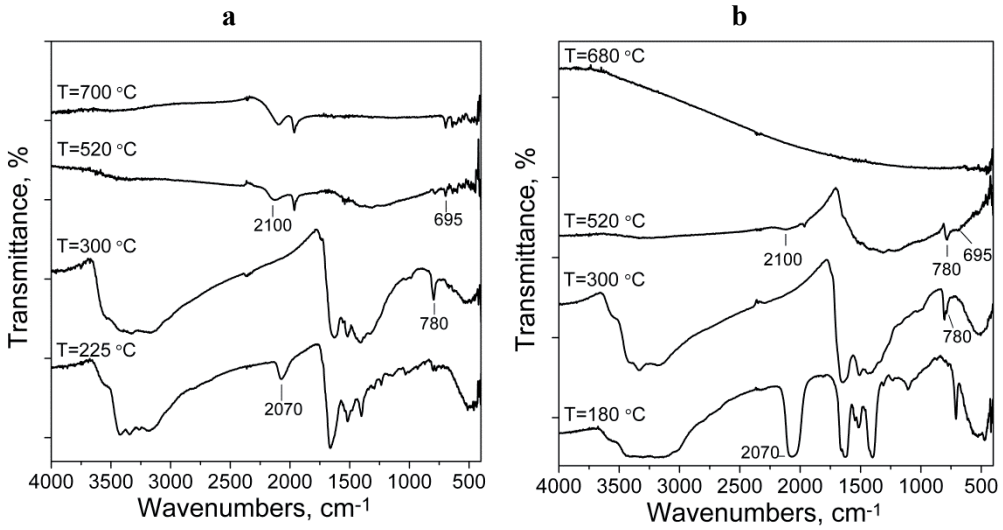

Fig. 3.17. FTIR spectra of solid intermediates of **1** (a) and **2** (b) heated at different temperatures with the heating rate of 10 °C/min in air in laboratory furnace.

Table 3.6. Crystalline decomposition products of **1** and **2**, as detected by *ex situ* XRD. Heat treatments were performed in a preparative scale in air in laboratory furnace

1 (In:S = 1:3)		**2** (In:S = 1:6)	
T, ºC	Main crystalline phases and JCPDS reference files	T, ºC	Main crystalline phases and JCPDS reference files
300	α-In_2S_3 (01-084-1385) ($InCl_3$ (00-034-1145))	300	α-In_2S_3 (01-084-1385)
410	β-In_2S_3 (01-074-7284) In_2O_3 (01-073-6440)	410	β-In_2S_3 (01-074-7284)
520	In_2O_3 (01-073-6440) $In_{2.24}(NCN)_3$ (00-051-0853) (β-In_2S_3 (01-074-7284))	520	In_2O_3 (01-073-6440) (β-In_2S_3 (01-074-7284))
700	In_2O_3 (01-073-6440) $In_{2.24}(NCN)_3$ (00-051-0853)	680	In_2O_3 (01-073-6440)
900	In_2O_3 (01-073-6440)	820	In_2O_3 (01-073-6440)

3.2.4 Reactions of thermal decomposition of precursors for In_2S_3 films

The thermal decomposition of **1** and **2** starts with the endothermic effects (around 200 °C) (Fig. 3.13) accompanied by the evolution of carbon disulfide (CS_2), ammonia (NH_3) and cyanamide (H_2NCN) at 210 °C from **1** (Figs. 3.16 and 3.14)

and at 200 °C from **2** (Fig. 3.14). Evolution of these three gases indicates the decomposition of adjacent thiourea ligands in the melt according to the reaction (Eq. 3.2) [118, 121, 122, 146, 147]:

$$2SC(NH_2)_{2(l)} = CS_{2(g)} + 2NH_{3(g)} + H_2NCN_{(l,g)} \qquad (3.2)$$

FTIR spectrum of the solid residues of **1** at 225 °C and of **2** at 180 °C (Fig. 3.17) show the vibration at 2070 cm^{-1} characteristic of both thiocyanate (SCN) and hydrogen bonded RNH_3^+ groups [119]. The presence of this peak indicates that probably part of $SC(NH_2)_2$ isomerized into ammonium thiocyanate (NH_4SCN), as it has also been observed during the thermal decomposition of different complex compounds, such as $Cd(SCN_2H_4)_2Cl_2$, $Zn(SCN_2H_4)_2Cl_2$, $Cu(SCN_2H_4)_3Cl$ [118 – 120], and $SC(NH_2)_2$ [147]. The isomerization of $SC(NH_2)_2$ could be presented as Eq. 3.3 [147]:

$$SC(NH_2)_{2(l)} + Heat = NH_4SCN_{(l)} \qquad (3.3)$$

The decomposition of both $SC(NH_2)_2$ and NH_4SCN could be responsible for the evolution of isothiocyanic acid (HNCS) and NH_3, as detected by EGA-FTIR in air (Fig. 3.14). Evolution of NH_3 in N_2 and in air was also confirmed by EGA-MS (Fig. 3.16). The release of HNCS and NH_3 could occur according to the reactions (Eq. 3.4, 3.5), as reported previously [118, 121].

$$NH_4SCN_{(l)} = HNCS_{(g)} + NH_{3(g)} \qquad (3.4)$$

$$SC(NH_2)_{2(l)} = HNCS_{(g)} + NH_{3(g)} \qquad (3.5)$$

The exothermic effects around 220 °C of **1** and **2** by the DTA curve (Fig. 3.13), followed closely the release of sulfur dioxide (SO_2) and carbonyl sulfide (COS) in air (Fig. 3.14). Interestingly, the release of SO_2 and COS was also detected from **1** in N_2 atmosphere (Fig. 3.16). The release of these gases imply to the oxidation of CS_2 vapor according to Eq. 3.6 [118, 121 – 123, 146]:

$$CS_{2(g)} + 1.5O_{2(g)} = SO_{2(g)} + COS_{(g)} \qquad (3.6)$$

The release of hydrogen cyanide (HCN) from **1** and **2** in air and also from **1** in N_2 atmosphere can be considered as the oxidation product of HNCS according to the reaction (Eq. 3.7) [118, 121, 123]:

$$HNCS_{(g)} + O_{2(g)} = HCN_{(g)} + SO_{2(g)} \qquad (3.7)$$

Formation of SO_2 and COS as oxidation products of CS_2; and HCN as the oxidation product of HNCS in inert atmosphere can result from either the oxygen contamination in **1** (a minute amount of urea inside used thiourea) or surroundings of the open measuring systems or a certain level of oxygen impurities are present in the inert purge gas used [146]. For example, Onishi et al. [148] pointed out that

although they used high purity argon for the thermal analysis, it still contained a small amount of oxygen (<10 ppm), which was responsible for the observed oxidation process. Furthermore, a small amount of oxygen (0.4 mass%) was detected in sample **1** by the EDX analysis performed on the Oxford Instruments INCA Energy system using the accelerating voltage of 7 kV in the Centre for Materials Research at Tallinn University of Technology (Tallinn, Estonia).

In addition to the reaction (Eq. 3.2), the evolution of H_2NCN at 240 °C in air (Fig. 3.14) might originate from the metal sulfide formation proposed by Krunks et al. [118]. The formation of In_2S_3 in the first decomposition step upon thermal decomposition of **1** and **2** in air is confirmed by XRD (Table 3.6). Thus, the reaction characterizing the formation of In_2S_3 can be assumed as follows (Eq. 3.8):

$$2InCl_{3(s)} + 3SC(NH_2)_{2(l)} = In_2S_{3(s)} + 3H_2NCN_{(l,g)} + 6HCl_{(g)} \quad (3.8)$$

H_2NCN vapors could condensate on the windows and mirrors of the IR gas cell, as it has been observed during the evolved gas analysis of the $Zn(SCN_2H_4)_2Cl_2$ [122], polymerization of H_2NCN is also possible [149]. This could be a reason why the first TG/DTA/EGA-FTIR experiment of **1** with the initial mass of 48.2 mg was canceled in the middle of the run as the jam in different parts of the measuring system occurred.

All of the above described gases evolve during the first mass loss step of **1** and **2** at temperatures below 300 °C. The FTIR spectra of the solid residues obtained by heating of **1** and **2** up to 300 °C in air still contain organic residues (Fig. 3.17). In the first decomposition step of **1** the mass losses were similar in N_2 and in air (33.9% and 34.8%, respectively), while for **2** the mass loss from the first step was 50.7%.

In the temperature interval of 300 – 400 °C in air, both **1** and **2** show endothermic decomposition reactions and evolution of NH_3, while the evolution of H_2NCN and HNCS were released only from **1** (Figs. 3.13 and 3.15). Probably an intermediate is formed in the first decomposition step, which at higher temperatures decomposes with the release of HNCS and NH_3, as also speculated in [147].

The FTIR spectrum of the solid product of **1** heated up to 520 °C (Fig. 3.17 a) shows vibrations at the 2100 and 695 cm^{-1} characteristic of the cyanamide group [119, 150]. According to XRD, the solid decomposition product of **1** at 520 °C contained crystalline phases of $In_{2.24}(NCN)_3$, In_2O_3 and traces of In_2S_3 (Table 3.6). Indium cyanamide is formed probably similarly to $ZnCN_2$ [119] by the reaction of H_2NCN and metal chloride (in the present case $InCl_3$, Eq. 3.9):

$$InCl_3 + H_2NCN \rightarrow In_{2.24}(NCN)_3 + HCl \uparrow \quad (3.9)$$

According to XRD, solid decomposition product of **2** at 520 °C comprises crystalline In_2O_3 and traces of In_2S_3, while crystalline $In_{2.24}(NCN)_3$ was not detected (Table 3.6).

In the third decomposition step (520 – 680 °C) of **1** in air the exothermic effect with maxima at 580 and 610 °C (Fig. 3.13) are accompanied by an evolution of

SO_2, and the release of CO_2 and H_2NCN with similar evolution profiles (Fig. 3.14). The evolution of CO_2 and H_2NCN indicate to the decomposition and combustion of organic pieces.

The release of SO_2 at around 600 °C from **1** was detected by EGA-FTIR in air (Fig. 3.14), EGA-MS shows the evolution of SO_2 also at around the same temperature in inert atmosphere (Fig. 3.16). The evolution of SO_2 is due to the oxidation of In_2S_3 according to Eq. 3.10

$$In_2S_{3(s)} + 4.5O_{2(g)} = In_2O_{3(s)} + 3SO_{2(g)} \qquad (3.10)$$

The oxidation of the In_2S_3 was confirmed by *ex situ* XRD, since solid decomposition product of **1** heated up to 700 °C contained only In_2O_3 and $In_{2.24}(NCN)_3$ phases (Table 3.6). Moreover, the *ex situ* FTIR study of the solid decomposition product of **1** at 700 °C in air (Fig. 3.17 a) indicates to the occurrence of the $In_{2.24}(NCN)_3$, which is in accordance with the XRD study.

For **2**, from the third step (400 – 680 °C) evolution profiles of H_2NCN and CO_2 show a monotonous increase without any distinct maxima and continuous evolution of HNCS (Fig. 3.14) with no maxima in the DTA curve (Fig. 3.13 b).

At temperatures above 700 °C up to the end of the decomposition process, the evolution of CO_2 and H_2NCN with strikingly similar profiles were recorded for **1** (both in N_2 and in air) and for **2** in air (Figs. 3.16 and 3.14). In addition, the continuous release of HNCS recorded from **2** in the temperature interval of 700 – 800 °C confirm further decomposition of an organic matter [143].

3.2.5 Summary on the formation and thermal analysis of precursors for In_2S_3 films

It has been shown that $InCl_3$ and $SC(NH_2)_2$ in the molar ratio of 1:3 (**1**) and 1:6 (**2**) in an aqueous solution interact to form a complex compound *mer*-trichlorotris(thiourea)-indium(III) ($In(tu)_3Cl_3$), where thiourea is coordinated to indium atom via sulfur atom, while in **2** free thiourea is also present. The thermal decomposition of both **1** and **2** results in In_2S_3 at temperatures below 300 °C.

The thermal decomposition of **1** took place in the temperature region of 205 – 750 °C in nitrogen atmosphere and in the temperature range of 205 – 730 °C in air. The thermal decomposition of **2** took place in the temperature interval of 180 – 790 °C. According to XRD, the final decomposition product of **1** and **2** in air was In_2O_3, whereas the final product of **1** in N_2 atmosphere contained In_2S_3 (92%) and In_2O_3 (8%). The total mass loss of **1** was higher than expected in both atmospheres, indicating release of some volatile indium species (e.g. $InCl_3$). The total mass loss of **2** in air was close to the theoretical value. The comparison of mass losses for **1** and **2** indicates that the excess of thiourea depresses the loss of indium from the system.

According to the thermoanalytical study, the possible reactions occurring during the thermal degradation of **1** and **2** in air are presented. It has been shown

that In_2S_3 forms in the first decomposition step from both, **1** and **2**, at temperatures below 300 °C according to the Eq. 3.8.

The thermal analysis study evidently showed that crystalline indium oxide from **2** in air came up at higher temperatures (around 500 °C) than that from **1** (at ca. 400 °C). Although the results of the thermoanalytical study cannot be transferred one-to-one to the film deposition procedure, it has been shown that the use of the precursor **2** can depress the formation of In_2O_3 phase in In_2S_3 films. It was experimentally confirmed with the results obtained from the study of the influence of different deposition parameters on the properties of In_2S_3 thin films deposited by the pneumatic CSP.

4. CONCLUSIONS

Resulting from the studies conducted in this thesis, the following conclusions on In_2S_3 deposition from spray solution containing $InCl_3$ and $SC(NH_2)_2$ by the chemical spray pyrolysis (CSP) process could be made:

1. Uniform and pin-hole free β-In_2S_3 thin films were grown at temperatures from 205 up to 365 °C (with aqueous spray solution) and up to 280 °C (with alcoholic spray solution), using $InCl_3$:$SC(NH_2)_2$ at molar ratios of 1:3 and 1:6 in the spray solution by the pneumatic spray pyrolysis method. The increase in the film growth temperature increased the crystallite size, and decreased the film thickness and chlorine content for all of the studied films.
2. The $InCl_3$:$SC(NH_2)_2$ molar ratio in the spray solution showed the following effects:
   - According to XPS, oxygen bounded to indium was detected in all sprayed films grown in the temperature range of 205 – 365 °C, but oxygen concentration was always higher in the films prepared from the $InCl_3$: $SC(NH_2)_2$ = 1:3 solution compared to those obtained by spray of the $InCl_3$: $SC(NH_2)_2$ = 1:6 solution. The use of the $InCl_3$: $SC(NH_2)_2$ = 1:6 solution leads to slightly larger crystallite size.
   - Noticeable effect on the bandgap and phase composition was observed for the films grown at $T_s \geq 365$ °C. E_g of 3.14 eV and 2.91 eV (direct transitions) are characteristic of the films sprayed from the $InCl_3$: $SC(NH_2)_2$ = 1:3 and 1:6 solutions, respectively. According to XRD, In_2O_3 phase is preferably formed in sprayed In_2S_3 films using the $InCl_3$: $SC(NH_2)_2$ = 1:3 solution. It was shown that formation of In_2O_3 phase is not due to the oxidation of the In_2S_3 phase at temperatures up to 450 °C.
3. It was shown that $InCl_3$ and $SC(NH_2)_2$ in an aqueous solution interact to form the complex compound mer-trichlorotris(thiourea)-indium(III) ($In(tu)_3Cl_3$). In this complex compound thiourea ligand is coordinated to the indium atom through the sulfur atom. $In(tu)_3Cl_3$ (**1**) is a single-source precursor for indium sulfide films in the CSP process using the spray solution with $InCl_3$:$SC(NH_2)_2$ at the molar ratio of 1:3. Using a solution with $InCl_3$:$SC(NH_2)_2$ at the molar ratio of 1:6, the dried precursor for In_2S_3 films is composed of the $In(tu)_3Cl_3$ and free, non-coordinated thiourea phases ($In(tu)_3Cl_3$ + 3tu, **2**).
4. The thermal decomposition of **1** took place in the temperature ranges of 205 – 730 °C and 205 – 750 °C in air and nitrogen atmospheres, respectively. The thermal decomposition of **1** in nitrogen and air consisted of three and four mass loss steps, respectively, with the total mass loss of 76.1 and 89.1%. The final decomposition product of **1** contained In_2S_3 (92%) and In_2O_3 (8%) in nitrogen atmosphere and In_2O_3 in air. For sample **1**, the total mass loss was higher than the theoretical mass loss in both

atmospheres, indicating the release of volatile indium containing species (e.g. $InCl_3$). The thermal decomposition of **2** in the temperature range of 180 – 790 °C in air showed four mass loss steps with a total mass loss of 78.5%. The final decomposition product of **2** in air was In_2O_3. The total mass loss of **2** was found to be close to the theoretical value, indicating that the excess of thiourea in the precursor hinders the release of volatile indium containing species from the system.

5. According to the evolved gas analysis by FTIR and MS, the gaseous species evolved during the decomposition of **1** and **2** in air include CS_2, NH_3, H_2NCN, HNCS, which upon oxidation form COS, SO_2, HCN and CO_2. The evolution of COS, SO_2, HCN and CO_2 were also detected during the decomposition of **1** in an inert atmosphere. This result and presence of In_2O_3 traces in In_2S_3, as the final decomposition product of **1** in an inert atmosphere, both refer that some oxygen contamination can be originated from the precursor.
6. The possible reactions of thermal decomposition of **1** and **2** were presented for each decomposition step taking into account the thermal effects, gases evolved and solid products of the decomposition. From both of the precursors, In_2S_3 is formed after the decomposition act of the complex compound, with the potential formation reaction (Eq. 3.8):

$$2InCl_{3(s)} + 3SC(NH_2)_{2(l)} = In_2S_{3(s)} + 3H_2NCN_{(l,g)} + 6HCl_{(g)}$$

7. Results of the current study allow us to produce the following recommendations for making In_2S_3 films by CSP: It should be taken into account that the formation of In_2S_3 films in CSP process passes through an intermediate complex compound, $In(tu)_3Cl_3$, formed in an aqueous solutions containing $InCl_3$ and $SC(NH_2)_2$ as starting chemicals. In_2S_3 forms upon thermal decomposition of $In(tu)_3Cl_3$ at temperatures ≥ 200 °C. The aqueous spray solution containing $InCl_3$ and $SC(NH_2)_2$ with the molar ratio of 1:6 and growth temperatures up to 400 °C can be used for the deposition of In_2S_3 films. The excess of thiourea in the spray solution compared to that required for the intermediate complex compound minimizes the formation of the In_2O_3 phase and depresses the loss of indium.

ACKNOWLEDGEMENTS

Firstly, I would like to thank my supervisor Leading Research Scientist Dr. Malle Krunks for inviting me into her study group, for her support and excellent guidance.

I also wish to thank Prof. Enn Mellikov, Head of the Department of Materials Science, for giving me opportunity to carry out my studies.

I want to thank Prof. Andres Öpik, Dean of the Faculty of Chemical and Materials Technology, for continuous support.

I am grateful to my colleagues Dr. Ilona Oja Açik, Dr. Arvo Mere, Dr. Tatjana Dedova and Dr. Atanas Katerski for their contribution to the work and all the other colleagues from the Laboratory of Thin Film Chemical Technologies for their help during my work. I want to thank Dr. Valdek Mikli and Dr. Olga Volobujeva for SEM and EDX analysis. Dr. Kaia Tõnsuaadu for TG/DTA/EGA-FTIR and to Dr. János Madarász are thanked for enabling co-operation for the TG/DTA/EGA-FTIR and TG/DTA/EGA-MS measurements and Dr. Petra Bombicz for single crystal XRD measurements. I would also like to thank MSc. Mati Danilson for XPS measurements and Dr. Karin Kerm for interesting and useful discussions. I thank MSc. Mare-Anne Laane for revising the language of the thesis.

This work is financially supported by the Estonian Ministry of Education and Research (Target Financing Project SF0140092s08); the Estonian Science Foundation under grants ETF6954, ETF7788 and ETF9081; Projects AR10128 (“New materials for solar energetics“) and AR12118 (“Efficient plasmonic absorbers for solar cells”); Centre of Excellence Mesosystems - Theory and Applications (Project TK114). This work has been partially supported by the Graduate School “Functional materials and technologies“ financed funding from the European Social Fund under project 1.2.0401.09-0079 in Estonia. Additionally, the Internationalization Programme DoRa Activity 8 for support is appreciated.

My warmest and sincere gratitude belongs to my husband Tauno, my son Tanel and to my parents Urmas and Reet for their unconditional support.

ABSTRACT

Indium sulfide (In_2S_3) thin films have been mainly used as buffer layer instead of CdS in chalcopyrite absorber layer based solar cells. In the literature, only limited number of studies have been reported on the deposition of In_2S_3 films by the pneumatic CSP. To our best knowledge, the chemistry of the In_2S_3 formation in the CSP process using $InCl_3$ and $SC(NH_2)_2$ (thiourea, tu) as starting chemicals has not been studied.

The objective of this thesis was to study the effect of the deposition parameter such as the growth temperature and the molar ratio of the starting chemicals ($InCl_3$ and $SC(NH_2)_2$) in aqueous or alcoholic solutions on the properties of In_2S_3 films prepared by the pneumatic CSP method. The films were characterized by means of XRD, SEM, EDX, UV-VIS and XPS methods. To study the formation of In_2S_3 in the CSP process, the intermediates formed in an aqueous spray solution with $InCl_3$:$SC(NH_2)_2$ molar ratios of 1:3 (named as **1**) and 1:6 (named as **2**) were determined. The thermal behavior of dried intermediates as precursors for In_2S_3 films was studied by applying the thermoanalytical methods (simultaneous TG/DTG/DTA coupled with EGA-FTIR and EGA-MS measurements) along with *ex situ* XRD and FTIR studies of solid products. The knowledge of formation chemistry of In_2S_3 in CSP process allows us to determine the optimal solution composition and thermal conditions of CSP and thereby control the properties of the sprayed In_2S_3 thin films.

In this study, In_2S_3 films were prepared by spraying the aqueous or alcoholic solutions containing $InCl_3$ and $SC(NH_2)_2$ as starting chemicals with molar ratios of 1:3 or 1:6 onto preheated glass sheets in air by varying the film growth temperatures (T_s) in the range of 205 – 410 °C. Results of the study showed that independent of $InCl_3$ and $SC(NH_2)_2$ molar ratio in the aqueous spray solution the films deposited at temperatures $T_s \leq 320$ °C are composed of the (0 0 12) orientated β-In_2S_3 films, which exhibited transparency over 70% in the visible spectral region, with E_g of 2.15 – 2.30 eV (indirect transitions) and ~2.90 eV (direct transitions). Use of the water-alcohol (1:1, by volume) based spray solutions instead of the aqueous ones results in significantly thinner and more compact In_2S_3 films with E_g of ~2.00 eV (indirect transitions) and E_g with 2.88 – 2.97 eV (direct transitions), when the films were grown at temperatures $T_s \leq 280$ °C. According to XPS, oxygen bounded to indium was detected in all sprayed films grown in the temperature range of 205 – 365 °C, but oxygen concentration was always higher in the films prepared from the spray solution with $InCl_3$: $SC(NH_2)_2$ at molar ratio of 1:3. Noticeable effect on the bandgap and phase composition was observed for the films grown at $T_s \geq 365$ °C. Moreover, it was shown that the formation of the In_2O_3 phase in the sprayed indium sulfide film grown at temperatures up to 450 °C is not due to the oxidation of In_2S_3.

It was shown that the $InCl_3$ and $SC(NH_2)_2$ with the molar ratio of 1:3 in an aqueous solution interact to form a complex compound mer-trichlorotris(thiourea)-indium(III) ($In(tu)_3Cl_3$), a single-source precursor for In_2S_3 films in the CSP process. Both **1** and **2** were containing an $In(tu)_3Cl_3$ complex compound, where $SC(NH_2)_2$ is coordinated to indium atom via sulfur atom; while in **2** also free $SC(NH_2)_2$ was present. The thermal decomposition of **1** took place in the

temperature range of 205 – 730 °C in air and in the range of 205 – 750 °C in nitrogen atmosphere with the total mass loss of 89.1% and 76.1%, respectively. The thermal degradation of **2** took place in the temperature interval of 180 – 790 °C with the total mass loss of 78.5%. The final decomposition product of **1** and **2** in air was In_2O_3, the final product of **1** in nitrogen contained In_2S_3 and residues of In_2O_3. The total mass loss of **1** was higher than the theoretical value (69.1%) in both atmospheres referring to the release of volatile indium species (e.g. $InCl_3$). The total mass loss of **2** was found to be close to the theoretical value, indicating that excess of thiourea in the precursor solution hinders the release of volatile indium species from the system. The gaseous species evolved during the decomposition of **1** and **2** include CS_2, NH_3, H_2NCN, HNCS, which upon their thermal oxidation form COS, SO_2, HCN and CO_2. From both of the precursors, In_2S_3 is formed below 300 °C, the crystalline In_2O_3 phase was detected in **1** at 410 °C and in **2** at 520 °C, while the crystalline $In_{2.24}(NCN)_3$ was found only in **1** at 520 – 700 °C in air by *ex situ* XRD. The reactions characteristic of each decomposition step are presented taking into account the thermal effects, gases evolved and the solid products of the decomposition.

According to the results obtained in the current thesis aqueous solutions containing $InCl_3$ and $SC(NH_2)_2$ as starting chemicals at the molar ratio of 1:6 and the growth temperatures below 400 °C are recommended for the deposition of β-In_2S_3 films by CSP. The excess of thiourea in the spray solution minimizes the formation of In_2O_3 phase and depresses the loss of indium compounds.

KOKKUVÕTE

In_2S_3 õhukesi kilesid kasutatakse päikeseenergeetikas puhverkihina CIS-tüüpi absorberiga päikesepatareides CdS asemel. Pneumaatilise keemilise pihustuspürolüüsi meetodil sadestatud In_2S_3 õhukeste kilede omadusi on vähe uuritud. Meile teadaolevalt pole seni uuritud In_2S_3 moodustumise keemiat pihustuspürolüüsi protsessis, kasutades lähteainetena $InCl_3$ ja $SC(NH_2)_2$ (tiokarbamiid, tu).

Käesolevas doktoritöös uuriti erinevate pihustusparameetrite nagu sadestustemperatuuri ja lähteainete ($InCl_3$ ja $SC(NH_2)_2$) molaarsuhte mõju vesilahusest või vee-alkoholi lahusest keemilise pihustuspürolüüsi meetodil sadestatud In_2S_3 õhukeste kilede omadustele. Kilede iseloomustamiseks kasutati XRD, SEM, EDX, UV-VIS ja XPS meetodeid. Samuti uuriti In_2S_3 moodustumist pihustuspürolüüsi protsessis. Selleks tehti kõigepealt kindlaks vaheühendid, mis moodustusid vesilahustes, kus $InCl_3$ ja $SC(NH_2)_2$ olid molaarsuhetel 1 : 3 (tähistatud kui **1**) ja 1 : 6 (tähistatud kui **2**). Kuivatatud pulbriliste vaheühendite ja nende termilise lagunemise uurimiseks rakendati termoanalüütiliste meetodite kompleksi (TG/DTG/DTA- koos EGA-FTIR- ja EGA-MS-analüüsiga) ja *ex situ* XRD- ning FTIR-analüüsi. In_2S_3 moodustumise protsessi keemia tundmine on vajalik, kuna see võimaldab leida optimaalsed termilised tingimused ja pihustuslahuse koostise, et seeläbi kontrollida sadestatud In_2S_3 kilede omadusi.

Kilede sadestamisel kasutati vesilahuseid või vee-alkoholi (suhe 1 : 1) lahuseid lähteainete $InCl_3$: $SC(NH_2)_2$ molaarsuhetel 1 : 3 või 1 : 6 ja sadestustemperatuure vahemikus 205–410 °C. Kõikides katsetes kasutati substraadina klaasi ja kandegaasina õhku. Leiti, et $T_s \leq 320$ °C sadestatud kiled, sõltumata lähteainete molaarsuhtest pihustatud vesilahustes, koosnevad (0 0 12) orienteeritud β-In_2S_3-kiledest, mille optiline läbilaskvus nähtava spektri osas on *ca* 70% ja E_g on vahemikus 2,15–2,30 eV (kaudsete üleminekute korral) ning ~2,90 eV (otseste üleminekute korral). Vee-alkoholi segu sisaldava pihustuslahusega sadestamisel $T_s \leq 280$ °C saadud In_2S_3-kiled on võrreldes vesilahustest sadestatud In_2S_3-kiledega õhemad ja kompaktsemad. Nende E_g on ~2,00 eV (kaudsete üleminekute korral) ning vahemikus 2,88 – 2,97 eV (otseste üleminekute korral). XPS-analüüsi järgi sisaldavad kõik vahemikus T_s = 205–365 °C sadestatud kiled indiumiga seotud hapnikku, kuid selle kogus on alati suurem kiledes, mille sadestamisel kasutati $InCl_3$ ja $SC(NH_2)_2$ molaarsuhet 1 : 3. Lähteainete molaarsuhte mõju optilise keelutsooni laiusele ja faasikoostisele ilmnes kiledes, mis on sadestatud vesilahustest $T_s \geq 365$ °C. Kile termiline järeltöötlus õhus näitas, et sulfiidi faasi oksüdatsioon mõjutab vähe In_2O_3 tekkimist kiles, mis on sadestatud kuni 450 °C juures.

Käesolevas töös näidati, et In_2S_3-kilede sadestamiseks keemilise pihustuspürolüüsi meetodil vesilahusest, mis sisaldab $InCl_3$ ja $SC(NH_2)_2$ molaarsuhtega 1 : 3 (**1**), moodustub kompleksühend mer-triklorotris(tiokarbamiid)-indium(III) ($In(tu)_3Cl_3$). **1** ja **2** koosnesid $In(tu)_3Cl_3$ kompleksühendist, milles kolm $SC(NH_2)_2$ molekuli on koordinatiivselt seotud indiumi katiooniga läbi väävli aatomi, lisaks sisaldas **2** ka vaba $SC(NH_2)_2$. **1** termiline lagunemine toimus temperatuuride vahemikus 205–730 °C õhus ja 205–750 °C lämmastiku keskkonnas summaarse massikaoga vastavalt 89,1% ja 76,1%. **2** termiline lagunemine toimus temperatuuride vahemikus 180–790 °C õhus

summaarse massikaoga 78,5%. **1** ja **2** termogravimeetrilise analüüsi lõpp-produkt õhus oli In_2O_3 ja **1** lõpp-produkt peale termogravimeetrilist analüüsi lämmastiku keskkonnas koosnes In_2S_3 (92%) ja In_2O_3 (8%) segust. Summaarne massikadu **1** korral oli oluliselt kõrgem teoreetiliselt arvutatud massikaost (69,1%), viidates termilise analüüsi käigus indiumi sisaldavate ühendite (nt $InCl_3$) lendumisele gaasi faasi. **2** puhul saadi sarnased summaarse massikao ja teoreetiliselt arvutatud massikao väärtused, mis näitab, et $SC(NH_2)_2$ liia korral on takistatud indiumi sisaldavate ühendite eraldumine. Lagunemisel eraldusid gaasilised produktid nagu CS_2, NH_3, H_2NCN, HNCS, COS, SO_2, HCN ja CO_2. Tahkete laguproduktide XRD-analüüsi järgi moodustus mõlemas (**1** ja **2**) In_2S_3 300 °C-st madalamatel temperatuuridel, kristalliline In_2O_3 moodustus **1** korral *ca* 410 °C ja **2** korral *ca* 520 °C juures, kuid vaid **1** korral leiti kristalliline $In_{2,24}(NCN)_3$ temperatuuride 520–700 °C juures. Igas lagunemisetapis toimuvad võimalikud keemilised reaktsioonid on esitatud, arvestades termilisi efekte, eralduvaid gaase ja tahkeid laguprodukte.

Töö tulemustest võib järeldada, et β-In_2S_3 õhukeste kilede sadestamisel keemilise pihustuspürolüüsi meetodil tuleb kasutada 400 °C-st madalamat sadestustemperatuuri ja lähtelahust, mis sisaldab $InCl_3$: $SC(NH_2)_2$ molaarsuhtel 1 : 6. $SC(NH_2)_2$ liig pihustuslahuses, võrreldes kogusega, mis on vajalik kompleksühendi moodustumiseks, vähendab In_2O_3 faasi moodustumist ja indiumiühendite kadu süsteemist.

REFERENCES

1. N. Barreau. Indium sulfide and relatives in the world of photovoltaics. – *Sol. Energy*, 2009, 83, p. 363 – 371.
2. S. Buecheler, D. Corica, D. Guettler, A. Chirila, R. Verma, U. Müller, T.P. Niesen, J. Palm, A.N. Tiwari. Ultrasonically sprayed indium sulfide buffer layers for Cu(In, Ga)(S, Se)$_2$ thin-film solar cells. – *Thin Solid Films*, 2009, 517, p. 2312 – 2315.
3. M. Krunks, E. Kärber, A. Katerski, K. Otto, I. Oja Acik, T. Dedova, A. Mere. Extremely thin absorber layer solar cells on zinc oxide nanorods by chemical spray. – *Sol. Energy Mater. Sol. Cells*, 2010, 94, p. 1191 – 1195.
4. D. Hariskos, S. Spiering, M. Powalla. Buffer layers in Cu(In,Ga)Se$_2$ solar cells and modules. – *Thin Solid Films*, 2005, 480 – 481, p. 99 – 109.
5. R. Lucena, I. Aguilera, P. Palacios, P. Wahnòn, J.C. Conesa. Synthesis and spectral properties of nanocrystalline V-substituted In_2S_3, a novel material for more efficient use of solar radiation. – *Chem. Mater*., 2008, 20, p. 5125 – 5127.
6. J.C. Conesa, R. Lucena, P. Wahnón, P. Palacios, J.J. Fernández, K. Sánchez, I. Aguilera. Photonic use of intermediate band materials on a chalcogenide-type semiconductor, IPC8 Class: AH01L31042FI, USPC Class: 136244 Patent application nr.: 20100206351, 19.08.2010.
7. К. Керм. Исследование условий получения фоточувствительных плёнок сульфида кадмия и его аналогов методом химического распыления: автореферат. Кандидата технических наук, Московский институт стали и сплавов, Таллинн, 1972.
8. A. Mere, Ph.D. Thesis. Structural and Electrical Properties of Spray Deposited Copper Indium Disulphide Films for Solar Cells. – Tallinn University of Technology, Estonia, 2006.
9. O. Kijatkina, Ph.D. Thesis. Deposition of Copper Indium Disulphide Films by Chemical Spray Pyrolysis. – Tallinn University of Technology, Estonia, 2004.
10. A. Katerski, Ph.D. Thesis. Chemical Composition of Sprayed Copper Indium Disulfide Films for Nanostructured Solar Cells. – Tallinn University of Technology, Estonia, 2011.
11. M. Krunks, O. Bijakina, T. Varema, V. Mikli, E. Mellikov. Structural and optical properties of sprayed $CuInS_2$ films. – *Thin Solid Films*, 1999, 338, p. 125 – 130.
12. T. Dedova, M. Krunks, O. Volobujeva, I. Oja. ZnS thin films deposited by spray pyrolysis technique. – *Phys. Stat. Sol. C*, 2005, 2, p. 1161 – 1166.
13. J. Hiie, T. Dedova, V. Valdna, K. Muska. Comparative study of nano-structured CdS thin films prepared by CBD and spray pyrolysis: Annealing effect, *Thin Solid Films*, 2006, 511 – 512, p. 443 – 447.
14. P. Pistor. Formation and Electronic Properties of In_2S_3/Cu(In,Ga)Se$_2$ Junctions and Related Thin Film Solar Cells Ph.D. Thesis, Freien Universität Berlin, Berlin, 2009.

15. T. Gödecke, K. Schubert. On the Phase Diagram InS_M. – *Zeitschrift für Metallkunde*, 1985, 76, p. 358 – 364.
16. Binary Alloy Phase Diagrams, edited by T. Massalski, P.R. Okamoto, P.R. Subramanian, L. Kacprzak. – ASM International, Materials Park (USA), Metals Park, OH : ASM, 1992, 3.
17. H. G. Ansell, R. S. Boorman. Phase Relationships in the In-S System. – *J. Eletrochem. Soc.: Solid State Sci.*, 1971, Volume 118, Issue 1, Pages 133 – 136.
18. W. Rehwald, G. Harbeke. On the conduction mechanism in single crystal β-indium sulfide In_2S_3. – *J. Phys. Chem. Solids*, 1965, 26, p. 1309 – 1318.
19. C.J.M. Rooymans. A New Type of Cation-Vacancy Ordering in the Spinel Lattice of In_2S_3. – *J. Inorg. Nucl. Chem*., 1959, 260, p. 78 – 79.
20. J. George, K.S. Joseph, B. Pradeep, T.I. Palson. Reactively Evaporated Films of Indium Sulphide. – *Phys. Stat. Sol. (a)*, 1988, 106, p. 123 – 131.
21. H. Hahn, W. Klingler. Über die Kristallstrukturen des In_2S_3 und In_2Te_3. – *Z. Anorg. Chemie*, 1949, 260, p. 97 – 109.
22. J.V. Landuyt, H. Hatwell, S. Amelinckx. The Domain Structure of β-In_2S_3 „Single Crystals“ due to the Ordering of Indium Vacancies. – *Mat. Res. Bull*., 1968, 3, p. 519 – 528.
23. R. Diehl, R. Nitsche. Vapour Growth of Three In_2S_3 Modifications by Iodine Transport. – *J. Cryst. Growth*, 1975, 28, p. 306 – 310.
24. International Centre for Diffraction Data (ICDD). Powder Diffraction, File (PDF), PDF-2 Release 2008.
25. K. Kambas, A. Anagnostopoulos, S. Ves, B. Ploss, J. Spyridelis. Optical Absorption Edge Investigation of $CdIn_2S_4$ and β-In_2S_3 Compounds. – *Phys. Stat. Sol. (b),* 1985, 127, 201 – 208.
26. H. Nakanishi, S. Endo, T. Irie. Fundamental Optical Absorption in Crystals of the $CdIn_2S_4$-In_2S_3 System. – *Japanese J. Appl. Phys*., 1980, 19, p. 261 – 266.
27. S.-H. Choe, T.-H. Bang, N.-O. Kim, H.-G. Kim, C.-I. Lee, M.-S. Jin, S.-K. Oh, W.-T. Kim. Optical properties of β-In_2S_3 and β-In_2S_3:Co^{2+} single crystals. – *Semicond. Sci. Technol.*, 2001, 16, p. 98 – 102.
28. W. Wang, W. Zhu, L. Zhang. A facile preparation and visible light-induced photocatalysis of indium sulfide superstructure. – *Res. Chem. Intermed*., 2009, 35, p. 761 – 767.
29. L. Song. Indium sulfide photocatalyst with visible light response and preparation method thereof. – Patent publication nr.: CN 101961655 A, 02.02.2011.
30. K. Tetsuya. Method for manufacturing hydrogen using photocatalyst. – Patent publication nr.: JP 2005–67973 A, 17.03.2005.
31. I. D. Aggarwal. Modified germanium sulfide glass. – Patent publication nr.: US 5629248, 13.03.1997
32. J.F. Trigo, B. Asenjo, J. Herrero, M.T. Gutiérrez. Optical characterization of In_2S_3 solar cell buffer layers grown by chemical bath and physical vapor deposition. – *Sol. Energy Mater. Sol. Cells*, 2008, 92, p. 1145 – 1148.

33. N. Barreau, S. Marsillac, J.C. Bernède, T. Ben Nasrallah, S. Belgacem. Optical Properties of Wide Band Gap Indium Sulphide Thin Films Obtained by Physical Vapor Deposition. – *Phys. Stat. Sol. (a)*, 2001, 184, p. 179 – 186.
34. D. Hariskos, R. Menner, S. Spiering, A. Eicke, M. Powalla, K. Ellmer, M. Oertel, B. Dimmler. In_2S_3 buffer layer deposited by magnetron sputtering for Cu(In-Ga)Se_2 sollar cells. *Proceedings of the 19th European Photovoltaic Solar Energy Conference*, 2004, p. 1894–1897.
35. D. Hariskos, R. Menner, E. Lotter, S. Spiering, M. Powalla. Magnetron sputtering of indium sulphide as the buffer layer in Cu(InGa)Se_2-based solar cells. *Proceedings of the 20th European Photovoltaic Solar Energy Conference*, 2005, p. 1713–1716.
36. N. Naghavi, R. Henriquez, V. Laptev, D. Lincot. Growth studies and characterisation of In_2S_3 thin films deposited by atomic layer deposition (ALD). – *Appl. Surf. Sci.,* 2004, 222, p. 65 – 73.
37. S. Spiering, D. Hariskos, S. Schrfder, M. Powalla. Stability behaviour of Cd-free Cu(In,Ga)Se_2 solar modules with In_2S_3 buffer layer prepared by atomic layer deposition. – *Thin Solid Films*, 2005, 480 – 481, p, 195 – 198.
38. B. Asenjo, A.M. Chaparro, M.T. Gutiérrez, J. Herrero, C. Maffiotte. Quartz crystal microbalance study of the growth of indium(III) sulphide films from a chemical solution. – *Electrochim. Acta*, 2004, 49, p. 737 – 744.
39. C. Kaufmann, S. Neve, W. Bohne, J. Klaer, R. Klenk, C. Pettenkofer, J. Röhrich, R. Scheer, U. Störkel, P.J. Dobson, *Proceedings of the 28th IEEE Photovoltaic Solar Energy Conference*, U.S.A., 2000, p. 688.
40. T. Dedova, J. Wienke, M. Goris, M. Krunks. Characterization of the chemical bath deposited $In(OH)_xS_y$ films: Effect of the growth conditions. – *Thin Solid Films*, 2007, 515, p. 6064 – 6067.
41. C. D. Lokhande, A. Ennaoui, P. S. Patil, M. Giersig, K. Diesner, M. Muller, H. Tributsch. Chemical bath deposition of indium sulphide thin films: preparation and characterization. – *Thin Solid Films*, 1999, 340, p. 18 – 23.
42. N.A. Allsop, A. Schönmann, A. Belaidi, H.-J. Muffler, B. Mertesacker, W. Bohne, E. Strub, J. Röhrich, M.C. Lux-Steiner, Ch.-H. Fischer. Indium sulfide thin films deposited by the spray ion layer gas reaction technique. – *Thin Solid Films*, 2006, 513, p. 52 – 56.
43. Y. Yasaki, N. Sonoyama, T. Sakata. Semiconductor sensitization of colloidal In_2S_3 on wide gap semiconductors. – *J. Electroanal. Chem*., 1999, 469, p. 116 – 122.
44. M. Kundakci, A. Ates, A. Astam, M. Yildirim. Structural, optical and electrical properties of CdS, $Cd_{0.5}In_{0.5}S$ and In_2S_3 thin films grown by SILAR method. – *Phys. E*, 2008, 40, p. 600 – 605.
45. R. Ranjith, Teny Theresa John, C. Sudha Kartha, K.P. Vijayakumar, T. Abe, Y. Kashiwab. Post-deposition annealing effect on In_2S_3 thin films deposited using SILAR technique. – *Mater. Sci. Semicon. Processing*, 2007, 10, p. 49 – 55.
46. W.-T. Kim, C.-D. Kim. Optical energy gaps of β-In_2S_3 thin films grown by spray pyrolysis. – *J. Appl. Phys*., 1986, 60, p. 2631 – 2633.

47. T.T. John, S. Bini, Y. Kashiwaba, T. Abe, Y. Yasuhiro, C. Sudha Kartha, K.P. Vijayakumar. Characterization of spray pyrolysed indium sulfide thin films. – *Semicond. Sci. Technol*., 2003, 18, p. 491 – 500.
48. M. Calixto-Rodriguez, A. Tiburcio-Silver, A. Ortiz, A. Sanchez-Juarez. Optoelectronical properties of indium sulfide thin films prepared by spray pyrolysis for photovoltaic applications. – *Thin Solid Films*, 2005, 29. 480 – 481, p. 133 – 137.
49. K. Ernits, D. Brémaud, S. Buecheler, C.J. Hibberd, M. Kaelin, G. Khrypunov, U. Müller, E. Mellikov, A.N. Tiwari. Characterisation of ultrasonically sprayed In_xS_y buffer layers for $Cu(In,Ga)Se_2$ solar cells. – *Thin Solid Films*, 2007, 515, p. 6051 – 6054.
50. N. Barreau, S. Marsillac, J.C. Bernède. Physico-chemical characterization of β-In_2S_3 thin films synthesized by solid-state reaction, induced by annealing, of the constituents sequentially deposited in thin layers. – *Vacuum*, 2000, 56, p. 101 – 106.
51. D. Abou-Ras, G. Kostorz, D. Hariskos, R. Menner, M. Powalla, S. Schorr, A.N. Tiwari. Structural and chemical analyses of sputtered In_xS_y buffer layers in $Cu(In,Ga)Se_2$ thin-film solar cells. – *Thin Solid Films*, 2009, 517, p. 2792 – 2798.
52. A. A. El Shazly, D. Abd. Elhady, H. S. Metwally, M. A. M. Seyam. Electrical properties of β-In_2S_3 thin films. – *J. Phys.: Condens. Matter*, 1998, 10, p. 5943 – 5954.
53. C. Guillén, T. Garíca, J. Herrero, M. T. Gutiérrez, F. Briones. Tailoring growth conditions for modulated flux deposition of In_2S_3 thin films. – *Thin Solid Films*, 2004, 451 –452, p. 112–115.
54. R. Yoosuf, M. Jayaraj. Optical and photoelectrical properties of β-In_2S_3 thin films prepared by two-stage process. – *Sol. En. Mat. Sol. Cells*, 2005, 89, p. 85 – 94.
55. J. Herrero, J. Ortega. n-Type In_2S_3 thin films prepared by gas chalcogenization of metallic electroplated indium: Photoelectrochemical characterization. – *Sol. Energy Mat.*, 1988, 17, p. 357 – 368.
56. J. Sterner, J. Malmström, L. Stolt. Study on ALD In_2S_3/$Cu(In,Ga)Se_2$ Interface Formation. – *Prog. Photovolt: Res. Appl*., 2005, 13, p. 179 – 193.
57. T. Asikainen, M. Ritala, M. Leskelä. Growth of In_2S_3 thin films by atomic layer epitaxy. – *Appl. Surf. Science*, 1994, 82 – 83, p. 122 – 125.
58. Yoshida, T., Yamaguchi, K., Toyoda, H., Akao, K., Sugiura, T., Minoura, H., Nosaka, Y., Chemical Bath Deposition of Band Gap Tailored Indium Sulfide Thin Films. – *Electrochem. Soc. Proc*., 1997, 97–20, p. 37 – 57.
59. R. Bayón, C. Guillén, M. A. Martínez, A. Martínez-Chaparro, M. T. Gutiérrez, J. Herrero. Different Substrates for Indium Hydroxy Sulphide Thin Films CBD-prepared. Approach to Large-area Deposition. – *Proceedings of the 2nd World Conference and Exhibition on Photovoltaic Solar Energy Conversion*, 1998, p. 636 – 639.
60. N. Bouguila, H. Bouzouita, E. Lacaze, A. Belhadj Amara, H. Bouchriha, A. Dhouib. Growth temperature effect on structural and morphological properties of "Spray" In_2S_3 thick films. – *J. Phys. III*, 1997, 7, p. 1647 –1660.

61. R. Bayón, C. Maffiotte, J. Herrero. Chemical bath deposition of indium hydroxy sulphide thin films: process and XPS characterization. – *Thin Solid Films*, 1999, 353, p. 100 – 107.
62. D. Hariskos, M. Ruckh, U. Rühle, T. Walter, H. Schock, J. Hedström, L. Stolt. A novel cadmium free buffer layer for $Cu(In,Ga)Se_2$ based solar cells. – *Sol. Energy Mater. Sol. Cells*, 1996, 41/42, p. 345 – 353.
63. N. Barreau, J.C. Bernède, S. Marsillac. Study of the new β-In_2S_3 containing Na thin films. Part II: Optical and electrical characterization of thin films. – *J. Cryst. Growth*, 2002, 241, p. 51 – 56.
64. N. Barreau, J.C. Bernède, H. El Maliki, S. Marsillac, X. Castel, J. Pinel. Recent studies on In_2S_3 containing oxygen thin films. – *Solid State Commun.*, 2002, 122, p. 445 – 450.
65. N. Barreau, J.C. Bernède, J. Kessler. Influence of oxygen, sodium and copper on the properties of PVD-grown indium sulfide. – *Proceeding of the 19th European Solar Energy Conference*, 2004, France p. 223 – 226.
66. N. Barreau, S. Marsillac, D. Albertini, J. C. Bernède. Structural, optical and electrical properties of β-$In_2S_{3-3x}O_{3x}$ thin films obtained by PVD. – *Thin Solid Films*, 2002, 403 – 404, p. 331 – 334.
67. D. Braunger, D. Hariskos, T. Walter, H.W. Schock. An 11.4% efficient polycrystalline thin film solar cell based on $CuInS_2$ with a Cd-free buffer layer. – *Sol. Energy Mater. Sol. Cells*, 1996, 40, p. 97 – 102.
68. N. Naghavi, D. Abou-Ras, N. Allsop, N. Barreau, S. Bücheler, A. Ennaoui, C.-H. Fischer, C. Guillen, D. Hariskos, J. Herrero, R. Klenk, K. Kushiya, D. Lincot, R. Menner, T. Nakada, C. Platzer-Björkman, S. Spiering, A.N. Tiwari, T. Törndahl. Buffer layers and transparent conducting oxides for chalcopyrite $Cu(In,Ga)(S,Se)_2$ based thin film photovoltaics: present status and current developments. – *Prog. Photovolt: Res. Appl.*, 2010, 18, p. 411 – 433.
69. N. Naghavi, S. Spiering, M. Powalla, B. Canava, D. Lincot. High-efficiency copper indium gallium diselenide (CIGS) solar cells with indium sulfide buffer layer deposited by atomic layer chemical vapor deposition (ALCVD). *Prog. Photovolt.: Res. Appl.*, 2003, 11, p. 437 – 443.
70. R. Sáez-Araoz, J. Krammer, S. Harndt, T. Koehler, M. Krueger, P. Pistor, A. Jasenek, F. Hergert, M. Ch. Lux-Steiner, C.-H. Fischer. ILGAR In_2S_3 buffer layers for Cd-free $Cu(In,Ga)(S,Se)_2$ solar cells with certified efficiencies above 16%. – *Prog. Photovolt.: Res. Appl*., 2012, DOI: 10.1002/pip.2268.
71. I. Repins, M. A. Contreras, B. Egaas, C. DeHart, J. Scharf, C. L. Perkins, B. To, R. Noufi. 19.9%-efficient ZnO/CdS/$CuInGaSe_2$ Solar Cell with 81.2% Fill Factor. – *Prog. Photovolt.: Res. Appl*., 2008, 16, p. 235 – 239.
72. P. Pistor, R. Caballero, D. Hariskos, V. Izquierdo-Roca, R. Wächter, S. Schorr, R. Klenk. Quality and stability of compound indium sulphide as source material for buffer layers in $Cu(In,Ga)Se_2$ solar cells. – *Sol. Energy Mater. Sol. Cells*, 2009, 93, p. 148 – 152.
73. A. Belaidi, Th. Dittrich, D. Kieven, J. Tornow, K. Schwarzburg, M. Kunst, N. Allsop, M.-Ch. Lux-Steiner, S. Gavrilov. ZnO-nanorod arrays for solar

cells with extremely thin sulfidic absorber. – *Sol. Energy Mater. Sol. Cells*, 2009, 93, p. 1033 – 1036.
74. D. Kieven, T. Dittrich, A. Belaidi, J. Tornow, K. Schwarzburg, N. Allsop, M.-C.h. Lux-Steiner. Effect of internal surface area on the performance of ZnO/In_2S_3/CuSCN solar cells with extremely thin absorber. – *Appl. Phys. Lett*., 2008, 92, p. 153107-1 – 153107-3.
75. M.S. Tomar, F.J. Garcia. Spray pyrolysis in solar cells and gas sensors. – *Prog. Cryst. Growth Charact.*, 1981, 4, p. 221 – 248.
76. P.S. Patil. Versatility of chemical spray pyrolysis technique. – *Mater. Chem. Phys*., 1999, 59, p. 185 – 198.
77. D. Perednis, L. J. Gauckler. Thin Film Deposition Using Spray Pyrolysis. – *J. Electroceramics*, 2005, 14, p. 103 – 111.
78. R.R. Chamberlein, J.S. Skarman. Chemical Spray Deposition Process for Inorganic Films. – *J. Electrochem. Soc.*, 1966, 113, p. 86 – 89.
79. J.B. Mooney, S.B. Radding. Spray Pyrolysis Processing. – *Ann. Rev. Mater. Sci*., 1982, 12, p. 81 – 101.
80. B. Elidrissi, M. Addou, M. Regragui, A. Bougrine, A. Kachouane, J.C. Bernède. Structure, composition and optical properties of ZnS thin films prepared by spray pyrolysis. – *Mater. Chem. Phys*., Volume 68, Issues 1–3, 15 February 2001, Pages 175 – 179.
81. M.A. Hernández-Fenollosa, M.C. López, V. Donderis, M. González, B. Marí, J.R. Ramos-Barrado, Role of precursors on morphology and optical properties of ZnS thin films prepared by chemical spray pyrolysis. – *Thin Solid Films*, 2008, 516, p. 1622 – 1625.
82. T.H. Sajeesh, Anita R. Warrier, C. Sudha Kartha, K.P. Vijayakumar. Optimization of parameters of chemical spray pyrolysis technique to get n and p-type layers of SnS. – *Thin Solid Films*, 2010, 518, p. 4370 – 4374.
83. S.-Y. Wang, W. Wang, Z.-H. Lu. Asynchronous-pulse ultrasonic spray pyrolysis deposition of Cu_xS (x=1, 2) thin films. – *Mater. Sci. Eng.*, 2003, B103, p. 184 – 188.
84. M.C. Baykul, A. Balcioglu. AFM and SEM studies of CdS thin films produced by an ultrasonic spray pyrolysis method. – *Microelectron. Eng.*, 2000, 51–52, p. 703 – 713.
85. R. Jayakrishnan, C. Sudha Kartha, K.P. Vijayakumar. Bias voltage controlled photoluminescence from β-In_2S_3 thin films. – *Mater. Sci. Semicond. Proc*., 2011, 14, p. 58 – 61.
86. A.A. Yadav, M.A. Barote, E.U. Masumdar. Studies on nanocrystalline cadmium sulphide (CdS) thin films deposited by spray pyrolysis. – *Sol. State Sci*., 2010, 12, p. 1173 – 1177.
87. Z. Zhao, V. Komin, V. Viswanathan, D. L. Morel, C. S. Ferekides, C.S. Application of tin-doped cadmium oxide films in CdTe/CdS solar cells. – *Proceedings of the 28th IEEE Photovoltaic Specialists Conference*, 2000, p. 662 – 665.
88. K.T. Ramakrishna Reddy, G.M. Shanthini, D. Johnston, R.W. Miles. Highly transparent and conducting CdO films grown by chemical spray pyrolysis. – *Thin Solid Films*, 2003, 427, p. 397 – 400.

89. K.H. Yoon, J.Y. Cho. Photoluminescence characteristics of zinc oxide thin films prepared by spray pyrolysis technique. – *Mater. Res. Bull.*, 2000, 35, p. 39 – 46.
90. S.J. Pearton, D.P. Norton, K. Ip, Y.W. Heo, T. Steiner. Recent progress in processing and properties of ZnO. – *Progr. Mater. Sci*., 2005, 50, p. 293 – 340.
91. V. Gokulakrishnan, S. Parthiban, K. Jeganathan and K. Ramamurthi. Investigations on the structural, optical and electrical properties of Nb-doped SnO_2 thin films. – *J. Mater. Sci*., 2011, 46, p. 5553 – 5558.
92. I. Oja, A. Mere, M. Krunks, R. Nisumaa, C.-H. Solterbeck, M. Es-Souni. Structural and electrical characterization of TiO_2 films grown by spray pyrolysis. – *Thin Solid Films*, 2006, 515, p. 674 – 677.
93. H. Z. Durusoy. Growth structures of MgO films on Si(100) and Si(111) surfaces. – J. *Mater. Sci. Letters*, 1991, 10. p. 1023 – 1025.
94. J.M. Bian, X.M. Li, T.L. Chen, X.D. Gao, W.D. Yu. Preparation of high quality MgO thin films by ultrasonic spray pyrolysis. – *Appl. Surf. Sci*., 2004, 228, p. 297 – 301.
95. S.P.S Arya, H.E.Hintermann, Growth of $YBa_2Cu_3O_{7-x}$ superconducting thin films by ultrasonic spray pyrolysis. – *Thin Solid Films*, 1990, 193, p. 841 – 846.
96. J.M. Grace, J.C.M. Marijnissen. A review of liquid atomization by electrical means. – *J. Aerosol. Sci*., 1994 25, p. 1005 – 1019.
97. H. Yoon, J.H. Woo, Y.M. Ra, S.S. Yoon, H.Y. Kim, S.J. Ahn, J.H. Yun, J. Gwak, K.H. Yoon, S.C. James. Electrostatic Spray Deposition of Copper–Indium Thin Films. – *Aerosol Sci. Techn*., 2011, 45, p. 1448 – 1455.
98. A. Nakaruk, C. C. Sorrell. Conceptual model for spray pyrolysis mechanism: fabrication and annealing of titania thin films. – *J. Coat. Technol. Res*., 2010, 7, p. 665 – 676.
99. M. Krunks, E. Mellikov. Zinc oxide thin films by the spray pyrolysis method. – *Thin Solid Films*. 1995, 270, p. 33 – 36.
100. M. Calixto-Rodriguez, H. Martinez, A. Sanchez-Juarez, J. Campos-Alvarez, A. Tiburcio-Silver, M.E. Calixto. Structural, optical, and electrical properties of tin sulfide thin films grown by spray pyrolysis. – *Thin Solid Films*, 2009, 517, p. 2497 – 2499.
101. M. Krunks, O. Kijatkina, H. Rebane, I. Oja, V. Mikli, A. Mere. Composition of $CuInS_2$ thin films prepared by spray pyrolysis. – *Thin Solid Films*, 2002, 403 – 404, p. 71 – 75.
102. A. Katerski, A. Mere, V. Kazlauskiene, J. Miskinis, A. Saar, L. Matisen, A. Kikas, M. Krunks. Surface analysis of spray deposited copper indium disulfide films. – *Thin Solid Films*, 2008, 516, p. 7110 – 7115.
103. L. Bhira, H. Essaidi, S. Belgacem, G. Couturier, J. Salardenne, N. Barreaux, J.C. Bernede. Structural and Photoelectrical Properties of Sprayed β-In_2S_3 Thin Films. – *Phys. Stat. Sol. (a)*, 2000, 181, p. 427 – 435.

104. T. Dedova, Ph.D. Thesis. Chemical Spray Pyrolysis Deposition of Zinc Sulfide Thin Films and Zinc Oxide Nanostructured Layers. – Tallinn University of Technology, Estonia, 2007.
105. I. Oja Açik, Ph.D. Thesis. Sol-gel deposition of titanium dioxide films. – Tallinn University of Technology, Estonia, 2007.
106. A.A. Yadav, E.U. Masumdar. Photoelectrochemical investigations of cadmium sulphide (CdS) thin film electrodes prepared by spray pyrolysis. – *J. Alloys Compd.*, 2011, 509 p. 5394 – 5399.
107. K. Ravichandran, P. Philominathan, Investigations on microstructural and optical properties of CdS films fabricated by a low-cost, simplified spray technique using perfume atomizer for solar cell applications. – *Sol. Energy*, 2008, 82, p. 1062 – 1066.
108. M.C. López, J.P. Espinos, F. Martín, D. Leinen, J.R. Ramos-Barrado, Growth of ZnS thin films obtained by chemical spray pyrolysis: The influence of precursors. – *J. Cryst. Growth*, 2005, 285, p. 66 – 75.
109. K.T. Ramakrishna Reddy, N. Koteswara Reddy, R.W. Miles. Photovoltaic properties of SnS based solar cells. – *Sol. Energy Mater. Sol. Cells*, 2006, 90, p. 3041 – 3046.
110. W.-Y. Kim, Balasaheb M. Palve, H. M. Pathan, O.-S. Joo. Spray pyrolytic deposition of polycrystalline Cu_2S thin films. – *Mater. Chem. Phys*., 2011, 131, p. 525 – 528.
111. L. Isac, A. Duta, A. Kriza, S. Manolache, M. Nanu. Copper sulfides obtained by spray pyrolysis - Possible absorbers in solid-state solar cells. – *Thin Solid Films*, 2007, 515, p. 5755 – 5758.
112. A.N. Tiwari, D. K. Pandya, K.L. Chopra. Fabrication and analysis of all-sprayed $CuInS_2$/ZnO solar cells. – *Sol. Cells*, 1987, 22, p. 263 – 273.
113. A. Katerski, M. Danilson, A. Mere, M. Krunks. Effect of the growth temperature on chemical composition of spray-deposited $CuInS_2$ thin films. – *Energy Procedia*, 2010, 2, p. 103 – 107.
114. C. Mahendran, N. Suriyanarayanan. Effect of temperature on structural, optical and photoluminescence properties of polycrystalline $CuInS_2$ thin films prepared by spray pyrolysis. – *Physica B: Condensed Matter*., 2010, 405, p. 2009 – 2013.
115. T. Sebastian, M. Gopinath, C. Sudha Kartha, K.P. Vijayakumar, T. Abe, Y. Kashiwaba. Role of substrate temperature in controlling properties of sprayed $CuInS_2$ absorbers. – *Sol. Energy*, 2009, 83, p. 1683 – 1688.
116. M. Krunks, E. Mellikov, E. Sork. Formation of CdS films by spray pyrolysis. – *Thin Solid Films*, 1986, 145, p. 105 – 109.
117. J. Madarász, P. Bombicz, M. Okuya, S. Kaneko. Thermal decomposition of thiourea complexes of Cu(I), Zn(II), and Sn(II) chlorides as precursors for the spray pyrolysis deposition of sulfide thin films. – *Sol. State Ion*., 2001, 141 – 142, p. 439 – 446.
118. M. Krunks, J. Madarász, L. Hiltunen, R. Mannonen, E. Mellikov, L. Niinistö. Structure and thermal behaviour of dichlorobis(thiourea) cadmium(II), a single-source precursor for CdS thin films. – *Acta Chem. Scand.*, 1997, 51, p. 294 – 301.

119. M. Krunks, J. Madarász, T. Leskelä, A. Mere, L. Niinistö, G. Pokol. Study of zinc thiocarbamide chloride, a single-source precursor for zinc sulfide thin films by spray pyrolysis. – *J. Therm. Anal. Calorim.*, 2003, 72, p. 497 – 506.
120. M. Krunks, T. Leskelä, I. Mutikainen, L. Niinistö. A thermoanalytical study of copper(I) thiocarbamide compounds. – *J. Therm. Anal. Calorim*., 1999, 56, p. 479 – 484.
121. M. Krunks, T. Leskelä, R. Mannonen, L. Niinistö. Thermal decomposition of copper(I) thiocarbamide chloride hemihydrate. – *J. Therm. Anal. Calorim*., 1998, 53, p. 355 – 364.
122. J. Madarász, M. Krunks, L. Niinistö, G. Pokol. Evolved gas analysis of dichlorobis(thiourea)zinc(II) by coupled TG-FTIR and TG/DTA-MS techniques. – *J. Therm. Anal. Calorim.*, 2004, 78, p. 679 – 686.
123. J. Madarász, P. Bombicz, M. Okuya, S. Kaneko, G. Pokol. Comparative online coupled TG-FTIR and TG/DTA-MS analyses of the evolved gases from thiourea complexes of $SnCl_2$ tetrachloropenta(thiourea) ditin(II), a compound rich in thiourea. – *J. Anal. Appl. Pyrolysis*, 2004, 72, p. 209 – 214.
124. M. Krunks, E. Mellikov, O. Bijakina. Intermediate compounds in formation of copper sulfides by spray pyrolysis. – *Proc. Estonian Acad. Sci. Eng.,* 1996, 2, p. 98 – 106.
125. P. Bombicz, I. Mutikainen, M. Krunks, T. Leskelä, J. Madarász, L. Niinistö. Synthesis, vibrational spectra and X-ray structures of copper(I) thiourea complexes. – *Inorg. Chim. Acta*, 2004, 357, p. 513 – 525.
126. P. Bombicz, J. Madarász, M. Krunks, L. Niinistö, G. Pokol. Multiple secondary interaction arrangement in the crystal structure of dichlorobis(thiourea-S)-zinc(II). – *J. Coord. Chem.*, 2007, 60, p. 457 – 464.
127. J. D. Donaldson, S. M. Grimes. X-ray crystal structure determinations of two thiourea tin(II) complexes: Diacetatobis(thiourea)tin(II) and ditin(II)tetrabromopenta(thiourea)dihydrate. – *Inorg. Chim. Acta*, 1984, 84, p. 173 – 177.
128. M. Krunks, E. Mellikov. Metal sulfide thin films by chemical spray pyrolysis. – *Proceedings of the SPIE*, 2001, 4415, p. 60 – 65.
129. T.T. John, C. Sudha Kartha, K.P. Vijayakumar, T. Abe, Y. Kashiwaba. Preparation of indium sulfide thin films by spray pyrolysis using a new precursor indium nitrate. – *Appl. Surf. Sci*., 2005, 252, p. 1360 – 1367.
130. H. Spasevska, C.C. Kitts, C. Ancora, G. Ruani. Optimised In_2S_3 thin films deposited by spray pyrolysis. – *Intern. J. Photoenergy*, 2012, Article ID 637943, 7 pages, doi:10.1155/2012/637943.
131. D. Corica, S. Buecheler, D. Guettler, A. Chirila, S. Seyrling, R. Verma and A. N. Tiwari. Indium Sulfide Buffer Layer for Cu(In,Ga)Se_2 Thin-Film Solar Cells Deposited by Ultrasonic Spray Pyrolysis. – *Proceeding of the 23rd European Photovoltaic Solar Energy Conference and Exhibition*, 2008, p. 2562 – 2565.

132. P.M. Ratheesh Kumar, T.T. John, C. Sudha Kartha, K.P. Vijayakumar. SHI induced modifications in spray pyrolysed β-In_2S_3 thin films. – *Nucl. Instrum. Met. Phys. Res. B*, 2006, 244, p. 171 – 173.
133. H.V. Rasika Dias. Indium and thallium. In: J. A. McCleverty, T. J. Meyer, editors. Comprehensive coordination chemistry II. Elsevier:Pergamon Press; 2003. p. 383 – 425.
134. R.L. Beddoes, D. Collison, F.E. Mabbs, J. Temperley. Structures of Trichlorobis(N,N,N',N'-tetramethylurea)indium(III) and Trichlorobis(N,N,N',N'-tetramethylthiourea)indium(III). – *Acta Crystallogr*., 1991, C47, p. 58 – 61.
135. A.J. Carty, D.G. Tuck. Co-ordination Compounds of Indium. Part I. Some Cationic Complexes of Indium (III). – *J. Chem. Soc*., 1964, p. 6012 – 6017.
136. M.A. Malyarik, A.B. Ilyukhin, S.P. Petrosyants, Y.A. Buslaev. Geometric isomers in indium(III) halo complexes: preparation and crystal structure of $[InCl_3(thio)_3]$. – *Zh. Neorg. Khim*., 1992, 37, p. 1504 – 1508.
137. P. O. Dunstan. Thermochemistry of some adducts of Indium(III) chloride with neutral donors. – *J. Therm. Anal. Calorim*., 2009, 97, p. 755 – 760.
138. G. Vazquez, E. Alvarez, J.M. Navaza. Surface Tension of Alcohol+Water from 20 to 50 °C. – *J. Chem. Eng. Data*, 1995, 40, p. 611 – 614.
139. R. Jayakrishnan, T. Sebastian, T.T. John, C. Sudha Kartha, K.P. Vijayakumar. Photoconductivity in sprayed β-In_2S_3 thin films under sub-band-gap excitation of 1.96 eV. – *J. Appl. Phys*., 2007, 102, p. 043109-1 – 043109-8.
140. A. Bourlange, D.J. Payne, R.G. Palgrave, J.S. Foord, R.G. Egdell, R.M.J. Jacobs, A. Schertel, J.L. Hutchison, P.J. Dobson. Investigation of the growth of In_2O_3 on Y-stabilized ZrO_2(100) by oxygen plasma assisted molecular beam epitaxy. – *Thin Solid Films*, 2009, 517, p. 4286 – 4294.
141. B. Asenjo, A.M. Chaparro, M.T. Gutiérrez, J. Herrero, J. Klaer. Study of $CuInS_2$/*buffer*/ZnO solar cells, with chemically deposited ZnS-In_2S_3 *buffer* layers. – *Thin Solid Films*, 2007, 515, p. 6036 – 6040.
142. C.D. Wagner, A.V. Naumkin, A. Kraut-Vass, J.W. Allison, C.J. Powell, J.R. Rumble Jr. NIST Standard Reference Database 20, Ver. 3.4, 2006 (Web Version at http://srdata.nist.gov/xps/index.htm).
143. G.M.S. El-Bahy, B.A. El-Sayed, A.A. Shabana. Vibrational and electronic studies on some metal thiourea complexes. – *Vib. Spectrosc*., 2003, 31, p. 101 – 107.
144. R. Rajasekaran, P.M. Ushasree, R. Jayavel, P. Ramasamy. Growth and characterization of zinc thiourea chloride (ZTC): a semiorganic nonlinear optical crystal. – *J. Cryst. Growth*, 2001, 229, p. 563 – 567.
145. B. Brunetti, V. Piacente, P. Scardala. A torsion study on the sublimation process of $InCl_3$. – *J. Chem. Eng. Data*. – 1998, 43, p. 101 – 104.
146. J. Madarász, G. Pokol. Comparative evolved gas analysis on thermal degradation of thiourea by coupled TG-FTIR and TG/DTA-MS instruments. – *J. Therm. Anal. Calorim*., 2007, 88, p. 329 – 336.

147. S. Wang, Q. Gao, J. Wang. Thermodynamic analysis of decomposition of thiourea and thiourea oxides. – *J. Phys. Chem. B*, 2005, 109, p. 17281 – 17289.
148. A. Onishi, P.S. Thomas, B.H. Stuart, J.P. Guerbois, S.L. Forbes. TG-MS analysis of the thermal decomposition of pig bone for forensic applications. – *J. Therm. Anal. Calorim*., 2008, 1, p. 87 – 90.
149. A. E. A. Porter, P. G. Sammes. Comprehensive organic chemistry, Oxford: Pergamon Press, 1979, vol. 4.
150. G. Baldinozzi, B. Malinowska, M. Rakib, G. Durand. Crystal structure and characterisation of cadmium cyanamide. – *J. Mater. Chem*., 2002, 12, p. 268 – 272.

Appendix A

Article I

K. Otto, A. Katerski, A. Mere, O. Volobujeva, M. Krunks. Spray Pyrolysis Deposition of Indium Sulfide Thin Films. Thin Solid Films, 2011, 519 (10), p. 3055 – 3060.

Appendix A

Article II

K. Otto, A. Katerski, O. Volobujeva, A. Mere, M. Krunks. Indium sulfide thin films deposited by chemical spray of aqueous and alcoholic solutions. Energy Procedia, 2011, 3, p. 63 – 69.

Appendix A

Article III

K. Otto, I. Oja Acik, K. Tõnsuaadu, A. Mere, M. Krunks. Thermoanalytical study of precursors for In_2S_3 thin films deposited by spray pyrolysis.– J. Therm. Anal. Calorim., 2011, 105 (2), p. 615 – 623.

Appendix A

Article IV

K. Otto, P. Bombicz, J. Madarász, I. Oja Acik, M. Krunks, G. Pokol. Structure and evolved gas analysis (TG/DTA-MS and TG-FTIR) of mer-triclorotris(thiourea)-indium(III), a precursor for indium sulfide thin films. J. Therm. Anal. Calorim., 2011, 105 (1), p. 83 – 91.

Appendix B

Curriculum Vitae

1. Isikuandmed

Ees- ja perekonnanimi	Kairi Otto
Sünniaeg ja -koht	10.05.1976, Tallinn
Kodakondsus	Eesti

2. Kontaktandmed

Telefon	+372 53 40 40 97
E-posti aadress	kairi.otto@gmail.com

3. Hariduskäik

Õppeasutus (nimetus lõpetamise ajal)	Lõpetamise aeg	Haridus (eriala/kraad)
Tallinna Tehnikaülikool	2001	Keemia- ja materjalitehnoloogia teaduskond, loodusteaduste magister
Tallinna Tehnikaülikool	1998	Keemia- ja materjalitehnoloogia teaduskond, insener
Tallinna Tondiraba Keskkool	1994	Keskharidus

4. Keelteoskus (alg-, kesk- või kõrgtase)

Keel	Tase
eesti keel	emakeel
inglise keel	kesktase
vene keel	kesktase
soome keel	kesktase
saksa keel	algtase

5. Täiendusõpe

2009 – …	Doktorikool "Funktsionaalsed materjalid ja tehnoloogiad", Tartu Ülikool ja Tallinna Tehnikaülikool
2012	MESO Tippkeskuse raames korraldatud konverents Tartu Ülikooli Füüsika Instituudis (22.05.2012)
2010	Uurimistöö, Anorgaanilise ja analüütilise keemia teaduskonnas Budapesti Tehnika- ja Majandusülikoolis, Ungari (november, 2010)
2002 – 2003	Täiendusõpe puidutehnoloogia alal, Puittoodete tehnoloogia teaduskond, Aalto Ülikool, Soome.

6. Kaitstud lõputööd

“Puidu adhesiooni parameetrite uurimine”, magistritöö, juhendaja Prof. Tiit Kaps

“Pinnaenergia mõõtmist mõjutavate tegurite uurimine”, diplomitöö, juhendajad Prof. Tiit Kaps ja Jüri-Aleksander Starkopf

7. Teadustöö põhisuunad

Protsessitehnoloogia ja materjaliteadus, materjalitehnoloogia

8. Teised uurimisprojektid

SF0140092s08 Õhukesekilelised ja nanostruktuursed materjalid keemilistel meetoditel (01.01.08 - 31.12.13)

TK114 Mesosüsteemide teooria ja rakendused (01.01.11 – 31.12.15)

AR12118 Efektiivsed plasmoonilised absorberid päikesepatareidele (01.07.12 – 31.12.14)

AR10128 Uued materjalid päikeseenergeetikale (01.07.10 – 31.08.15)

ETF9081 Absorberkihid keemilise pihustuspürolüüsi meetodil nanostruktuursetele päikesepatareidele (01.01.12 – 31.12.15)

ETF7788 Sool-geeli meetodil kasvatatud metalli oksiidide kihid optoelektroonikale (01.01.09 – 31.12.12)

Appendix B

Curriculum Vitae

1. Personal data

Name	Kairi Otto
Date and place of birth	10.05.1976 Tallinn
Citizenship	Estonian

2. Contact information

Phone	+372 53 40 40 97
E-mail	kairi.otto@gmail.com

3. Education

Educational institution	Graduation year	Education (field of study/degree)
Tallinn University of Technology	2001	Faculty of Chemical and Materials Technology, Master's Degree in Natural Sciences
Tallinn University of Technology	1998	Faculty of Chemical and Materials Technology, graduated engineer
Tallinn Tondiraba High School	1994	High school education

4. Language competence/skills (fluent; average, basic skills)

Language	Level
Estonian	Fluent
English	Average
Russian	Average
Finnish	Average
German	Basic skills

5. Special Courses

2009 – …	Graduate School "Functional Materials and Technologies" University of Tartu and Tallinn University of Technology.
2012	Project meeting of Centre of Excellence Mesosystems – Theory and Applications, University of Tartu (22.05.2012).

2010	Research in Department of Inorganic and Analytical Chemistry, Budapest, University of Technology and Economics Hungary (November, 2010).
2002 – 2003	Exchange student in Department of Forest Products Technology, Aalto University, Finland.

6. Defended theses

"Study of wood adhesion parameters", master thesis, supervisor Prof. Tiit Kaps

"Study of factors influencing the surface energy measurements", diploma work, supervisors Prof. Tiit Kaps and Jüri-Aleksander Starkopf

7. Main areas of scientific work/Current research topics

Natural Sciences and Engineering, Process Technology and Materials Science, Materials Technology

8. Other research projects

SF0140092s08 Thin film and nanostructured materials by chemical methods (01.01.08 – 31.12.13)

TK114 Mesosystems – Theory and Applications (01.01.11 – 31.12.15)

AR12118 Efficient plasmonic absorbers for solar cells (01.07.12 – 31.12.14)

AR10128 New materials for solar energetics (01.07.10 – 31.08.15)

ETF9081 Absorber layers by chemical spray pyrolysis for nanostructured solar cells (01.01.12 – 31.12.15)

ETF7788 Deposition of sol-gel derived metal oxide layers for optoelectronics (01.01.09 – 31.12.12)

DISSERTATIONS DEFENDED AT TALLINN UNIVERSITY OF TECHNOLOGY ON *NATURAL AND EXACT SCIENCES*

1. **Olav Kongas**. Nonlinear Dynamics in Modeling Cardiac Arrhytmias. 1998.

2. **Kalju Vanatalu**. Optimization of Processes of Microbial Biosynthesis of Isotopically Labeled Biomolecules and Their Complexes. 1999.

3. **Ahto Buldas**. An Algebraic Approach to the Structure of Graphs. 1999.

4. **Monika Drews**. A Metabolic Study of Insect Cells in Batch and Continuous Culture: Application of Chemostat and Turbidostat to the Production of Recombinant Proteins. 1999.

5. **Eola Valdre**. Endothelial-Specific Regulation of Vessel Formation: Role of Receptor Tyrosine Kinases. 2000.

6. **Kalju Lott**. Doping and Defect Thermodynamic Equilibrium in ZnS. 2000.

7. **Reet Koljak**. Novel Fatty Acid Dioxygenases from the Corals *Plexaura homomalla* and *Gersemia fruticosa.* 2001.

8. **Anne Paju**. Asymmetric oxidation of Prochiral and Racemic Ketones by Using Sharpless Catalyst. 2001.

9. **Marko Vendelin**. Cardiac Mechanoenergetics *in silico*. 2001.

10. **Pearu Peterson**. Multi-Soliton Interactions and the Inverse Problem of Wave Crest. 2001.

11. **Anne Menert**. Microcalorimetry of Anaerobic Digestion. 2001.

12. **Toomas Tiivel**. The Role of the Mitochondrial Outer Membrane in *in vivo* Regulation of Respiration in Normal Heart and Skeletal Muscle Cell. 2002.

13. **Olle Hints**. Ordovician Scolecodonts of Estonia and Neighbouring Areas: Taxonomy, Distribution, Palaeoecology, and Application. 2002.

14. **Jaak Nõlvak**. Chitinozoan Biostratigrapy in the Ordovician of Baltoscandia. 2002.

15. **Liivi Kluge**. On Algebraic Structure of Pre-Operad. 2002.

16. **Jaanus Lass**. Biosignal Interpretation: Study of Cardiac Arrhytmias and Electromagnetic Field Effects on Human Nervous System. 2002.

17. **Janek Peterson**. Synthesis, Structural Characterization and Modification of PAMAM Dendrimers. 2002.

18. **Merike Vaher**. Room Temperature Ionic Liquids as Background Electrolyte Additives in Capillary Electrophoresis. 2002.

19. **Valdek Mikli**. Electron Microscopy and Image Analysis Study of Powdered Hardmetal Materials and Optoelectronic Thin Films. 2003.

20. **Mart Viljus**. The Microstructure and Properties of Fine-Grained Cermets. 2003.

21. **Signe Kask**. Identification and Characterization of Dairy-Related *Lactobacillus.* 2003

22. **Tiiu-Mai Laht**. Influence of Microstructure of the Curd on Enzymatic and Microbiological Processes in Swiss-Type Cheese. 2003.

23. **Anne Kuusksalu**. 2–5A Synthetase in the Marine Sponge *Geodia cydonium*. 2003.

24. **Sergei Bereznev**. Solar Cells Based on Polycristalline Copper-Indium Chalcogenides and Conductive Polymers. 2003.

25. **Kadri Kriis**. Asymmetric Synthesis of C_2-Symmetric Bimorpholines and Their Application as Chiral Ligands in the Transfer Hydrogenation of Aromatic Ketones. 2004.

26. **Jekaterina Reut**. Polypyrrole Coatings on Conducting and Insulating Substracts. 2004.

27. **Sven Nõmm**. Realization and Identification of Discrete-Time Nonlinear Systems. 2004.

28. **Olga Kijatkina**. Deposition of Copper Indium Disulphide Films by Chemical Spray Pyrolysis. 2004.

29. **Gert Tamberg**. On Sampling Operators Defined by Rogosinski, Hann and Blackman Windows. 2004.

30. **Monika Übner**. Interaction of Humic Substances with Metal Cations. 2004.

31. **Kaarel Adamberg**. Growth Characteristics of Non-Starter Lactic Acid Bacteria from Cheese. 2004.

32. **Imre Vallikivi**. Lipase-Catalysed Reactions of Prostaglandins. 2004.

33. **Merike Peld**. Substituted Apatites as Sorbents for Heavy Metals. 2005.

34. **Vitali Syritski**. Study of Synthesis and Redox Switching of Polypyrrole and Poly(3,4-ethylenedioxythiophene) by Using *in-situ* Techniques. 2004.

35. **Lee Põllumaa**. Evaluation of Ecotoxicological Effects Related to Oil Shale Industry. 2004.

36. **Riina Aav**. Synthesis of 9,11-Secosterols Intermediates. 2005.

37. **Andres Braunbrück**. Wave Interaction in Weakly Inhomogeneous Materials. 2005.

38. **Robert Kitt**. Generalised Scale-Invariance in Financial Time Series. 2005.

39. **Juss Pavelson**. Mesoscale Physical Processes and the Related Impact on the Summer Nutrient Fields and Phytoplankton Blooms in the Western Gulf of Finland. 2005.

40. **Olari Ilison**. Solitons and Solitary Waves in Media with Higher Order Dispersive and Nonlinear Effects. 2005.

41. **Maksim Säkki**. Intermittency and Long-Range Structurization of Heart Rate. 2005.

42. **Enli Kiipli**. Modelling Seawater Chemistry of the East Baltic Basin in the Late Ordovician–Early Silurian. 2005.

43. **Igor Golovtsov**. Modification of Conductive Properties and Processability of Polyparaphenylene, Polypyrrole and polyaniline. 2005.

44. **Katrin Laos**. Interaction Between Furcellaran and the Globular Proteins (Bovine Serum Albumin β-Lactoglobulin). 2005.

45. **Arvo Mere**. Structural and Electrical Properties of Spray Deposited Copper Indium Disulphide Films for Solar Cells. 2006.

46. **Sille Ehala**. Development and Application of Various On- and Off-Line Analytical Methods for the Analysis of Bioactive Compounds. 2006.

47. **Maria Kulp**. Capillary Electrophoretic Monitoring of Biochemical Reaction Kinetics. 2006.

48. **Anu Aaspõllu.** Proteinases from *Vipera lebetina* Snake Venom Affecting Hemostasis. 2006.

49. **Lyudmila Chekulayeva**. Photosensitized Inactivation of Tumor Cells by Porphyrins and Chlorins. 2006.

50. **Merle Uudsemaa**. Quantum-Chemical Modeling of Solvated First Row Transition Metal Ions. 2006.

51. **Tagli Pitsi**. Nutrition Situation of Pre-School Children in Estonia from 1995 to 2004. 2006.

52. **Angela Ivask**. Luminescent Recombinant Sensor Bacteria for the Analysis of Bioavailable Heavy Metals. 2006.

53. **Tiina Lõugas**. Study on Physico-Chemical Properties and Some Bioactive Compounds of Sea Buckthorn (*Hippophae rhamnoides* L.). 2006.

54. **Kaja Kasemets**. Effect of Changing Environmental Conditions on the Fermentative Growth of *Saccharomyces cerevisae* S288C: Auxo-accelerostat Study. 2006.

55. **Ildar Nisamedtinov**. Application of ^{13}C and Fluorescence Labeling in Metabolic Studies of *Saccharomyces* spp. 2006.

56. **Alar Leibak**. On Additive Generalisation of Voronoï's Theory of Perfect Forms over Algebraic Number Fields. 2006.

57. **Andri Jagomägi**. Photoluminescence of Chalcopyrite Tellurides. 2006.

58. **Tõnu Martma**. Application of Carbon Isotopes to the Study of the Ordovician and Silurian of the Baltic. 2006.

59. **Marit Kauk**. Chemical Composition of $CuInSe_2$ Monograin Powders for Solar Cell Application. 2006.

60. **Julia Kois**. Electrochemical Deposition of $CuInSe_2$ Thin Films for Photovoltaic Applications. 2006.

61. **Ilona Oja Açik**. Sol-Gel Deposition of Titanium Dioxide Films. 2007.

62. **Tiia Anmann**. Integrated and Organized Cellular Bioenergetic Systems in Heart and Brain. 2007.

63. **Katrin Trummal**. Purification, Characterization and Specificity Studies of Metalloproteinases from *Vipera lebetina* Snake Venom. 2007.

64. **Gennadi Lessin**. Biochemical Definition of Coastal Zone Using Numerical Modeling and Measurement Data. 2007.

65. **Enno Pais**. Inverse problems to determine non-homogeneous degenerate memory kernels in heat flow. 2007.

66. **Maria Borissova**. Capillary Electrophoresis on Alkylimidazolium Salts. 2007.

67. **Karin Valmsen**. Prostaglandin Synthesis in the Coral *Plexaura homomalla*: Control of Prostaglandin Stereochemistry at Carbon 15 by Cyclooxygenases. 2007.

68. **Kristjan Piirimäe**. Long-Term Changes of Nutrient Fluxes in the Drainage Basin of the Gulf of Finland – Application of the PolFlow Model. 2007.

69. **Tatjana Dedova**. Chemical Spray Pyrolysis Deposition of Zinc Sulfide Thin Films and Zinc Oxide Nanostructured Layers. 2007.

70. **Katrin Tomson**. Production of Labelled Recombinant Proteins in Fed-Batch Systems in *Escherichia coli*. 2007.

71. **Cecilia Sarmiento**. Suppressors of RNA Silencing in Plants. 2008.

72. **Vilja Mardla**. Inhibition of Platelet Aggregation with Combination of Antiplatelet Agents. 2008.

73. **Maie Bachmann**. Effect of Modulated Microwave Radiation on Human Resting Electroencephalographic Signal. 2008.

74. **Dan Hüvonen**. Terahertz Spectroscopy of Low-Dimensional Spin Systems. 2008.

75. **Ly Villo**. Stereoselective Chemoenzymatic Synthesis of Deoxy Sugar Esters Involving *Candida antarctica* Lipase B. 2008.

76. **Johan Anton**. Technology of Integrated Photoelasticity for Residual Stress Measurement in Glass Articles of Axisymmetric Shape. 2008.

77. **Olga Volobujeva**. SEM Study of Selenization of Different Thin Metallic Films. 2008.

78. **Artur Jõgi**. Synthesis of 4'-Substituted 2,3'-dideoxynucleoside Analogues. 2008.

79. **Mario Kadastik**. Doubly Charged Higgs Boson Decays and Implications on Neutrino Physics. 2008.

80. **Fernando Pérez-Caballero**. Carbon Aerogels from 5-Methylresorcinol-Formaldehyde Gels. 2008.

81. **Sirje Vaask**. The Comparability, Reproducibility and Validity of Estonian Food Consumption Surveys. 2008.

82. **Anna Menaker**. Electrosynthesized Conducting Polymers, Polypyrrole and Poly(3,4-ethylenedioxythiophene), for Molecular Imprinting. 2009.

83. **Lauri Ilison**. Solitons and Solitary Waves in Hierarchical Korteweg-de Vries Type Systems. 2009.

84. **Kaia Ernits**. Study of In_2S_3 and ZnS Thin Films Deposited by Ultrasonic Spray Pyrolysis and Chemical Deposition. 2009.

85. **Veljo Sinivee**. Portable Spectrometer for Ionizing Radiation "Gammamapper". 2009.

86. **Jüri Virkepu**. On Lagrange Formalism for Lie Theory and Operadic Harmonic Oscillator in Low Dimensions. 2009.

87. **Marko Piirsoo**. Deciphering Molecular Basis of Schwann Cell Development. 2009.

88. **Kati Helmja**. Determination of Phenolic Compounds and Their Antioxidative Capability in Plant Extracts. 2010.

89. **Merike Sõmera**. Sobemoviruses: Genomic Organization, Potential for Recombination and Necessity of P1 in Systemic Infection. 2010.

90. **Kristjan Laes**. Preparation and Impedance Spectroscopy of Hybrid Structures Based on $CuIn_3Se_5$ Photoabsorber. 2010.

91. **Kristin Lippur**. Asymmetric Synthesis of 2,2'-Bimorpholine and its 5,5'-Substituted Derivatives. 2010.

92. **Merike Luman**. Dialysis Dose and Nutrition Assessment by an Optical Method. 2010.

93. **Mihhail Berezovski**. Numerical Simulation of Wave Propagation in Heterogeneous and Microstructured Materials. 2010.

94. **Tamara Aid-Pavlidis**. Structure and Regulation of BDNF Gene. 2010.

95. **Olga Bragina**. The Role of Sonic Hedgehog Pathway in Neuro- and Tumorigenesis. 2010.

96. **Merle Randrüüt**. Wave Propagation in Microstructured Solids: Solitary and Periodic Waves. 2010.

97. **Marju Laars**. Asymmetric Organocatalytic Michael and Aldol Reactions Mediated by Cyclic Amines. 2010.

98. **Maarja Grossberg**. Optical Properties of Multinary Semiconductor Compounds for Photovoltaic Applications. 2010.

99. **Alla Maloverjan**. Vertebrate Homologues of Drosophila Fused Kinase and Their Role in Sonic Hedgehog Signalling Pathway. 2010.

100. **Priit Pruunsild**. Neuronal Activity-Dependent Transcription Factors and Regulation of Human *BDNF* Gene. 2010.

101. **Tatjana Knjazeva**. New Approaches in Capillary Electrophoresis for Separation and Study of Proteins. 2011.

102. **Atanas Katerski**. Chemical Composition of Sprayed Copper Indium Disulfide Films for Nanostructured Solar Cells. 2011.

103. **Kristi Timmo.** Formation of Properties of $CuInSe_2$ and $Cu_2ZnSn(S,Se)_4$ Monograin Powders Synthesized in Molten KI. 2011.

104. **Kert Tamm**. Wave Propagation and Interaction in Mindlin-Type Microstructured Solids: Numerical Simulation. 2011.

105. **Adrian Popp**. Ordovician Proetid Trilobites in Baltoscandia and Germany. 2011.

106. **Ove Pärn**. Sea Ice Deformation Events in the Gulf of Finland and This Impact on Shipping. 2011.

107. **Germo Väli**. Numerical Experiments on Matter Transport in the Baltic Sea. 2011.

108. **Andrus Seiman**. Point-of-Care Analyser Based on Capillary Electrophoresis. 2011.

109. **Olga Katargina**. Tick-Borne Pathogens Circulating in Estonia (Tick-Borne Encephalitis Virus, *Anaplasma phagocytophilum*, *Babesia* Species): Their Prevalence and Genetic Characterization. 2011.

110. **Ingrid Sumeri**. The Study of Probiotic Bacteria in Human Gastrointestinal Tract Simulator. 2011.

111. **Kairit Zovo**. Functional Characterization of Cellular Copper Proteome. 2011.

112. **Natalja Makarytsheva**. Analysis of Organic Species in Sediments and Soil by High Performance Separation Methods. 2011.
113. **Monika Mortimer**. Evaluation of the Biological Effects of Engineered Nanoparticles on Unicellular Pro- and Eukaryotic Organisms. 2011.
114. **Kersti Tepp**. Molecular System Bioenergetics of Cardiac Cells: Quantitative Analysis of Structure-Function Relationship. 2011.
115. **Anna-Liisa Peikolainen**. Organic Aerogels Based on 5-Methylresorcinol. 2011.
116. **Leeli Amon**. Palaeoecological Reconstruction of Late-Glacial Vegetation Dynamics in Eastern Baltic Area: A View Based on Plant Macrofossil Analysis. 2011.
117. **Tanel Peets**. Dispersion Analysis of Wave Motion in Microstructured Solids. 2011.
118. **Liina Kaupmees**. Selenization of Molybdenum as Contact Material in Solar Cells. 2011.
119. **Allan Olspert**. Properties of VPg and Coat Protein of Sobemoviruses. 2011.
120. **Kadri Koppel**. Food Category Appraisal Using Sensory Methods. 2011.
121. **Jelena Gorbatšova**. Development of Methods for CE Analysis of Plant Phenolics and Vitamins. 2011.
122. **Karin Viipsi**. Impact of EDTA and Humic Substances on the Removal of Cd and Zn from Aqueous Solutions by Apatite. 2012.
123. **David Schryer**. Metabolic Flux Analysis of Compartmentalized Systems Using Dynamic Isotopologue Modeling. 2012.
124. **Ardo Illaste**. Analysis of Molecular Movements in Cardiac Myocytes. 2012.
125. **Indrek Reile**. 3-Alkylcyclopentane-1,2-Diones in Asymmetric Oxidation and Alkylation Reactions. 2012.
126. **Tatjana Tamberg**. Some Classes of Finite 2-Groups and Their Endomorphism Semigroups. 2012.
127. **Taavi Liblik**. Variability of Thermohaline Structure in the Gulf of Finland in Summer. 2012.
128. **Priidik Lagemaa**. Operational Forecasting in Estonian Marine Waters. 2012.
129. **Andrei Errapart**. Photoelastic Tomography in Linear and Non-linear Approximation. 2012.
130. **Külliki Krabbi**. Biochemical Diagnosis of Classical Galactosemia and Mucopolysaccharidoses in Estonia. 2012.
131. **Kristel Kaseleht**. Identification of Aroma Compounds in Food using SPME-GC/MS and GC-Olfactometry. 2012.
132. **Kristel Kodar**. Immunoglobulin G Glycosylation Profiling in Patients with Gastric Cancer. 2012.
133. **Kai Rosin**. Solar Radiation and Wind as Agents of the Formation of the Radiation Regime in Water Bodies. 2012.
134. **Ann Tiiman**. Interactions of Alzheimer`s Amyloid-Beta Peptides with Zn(II) and Cu(II) Ions. 2012.
135. **Olga Gavrilova**. Application and Elaboration of Accounting Approaches for Sustainable Development. 2012.
136. **Olesja Bondarenko**. Development of Bacterial Biosensors and Human Stem Cell-Based *In Vitro* Assays for the Toxicological Profiling of Synthetic Nanoparticles. 2012.
137. **Katri Muska**. Study of Composition and Thermal Treatments of Quaternary Compounds for Monograin Layer Solar Cells. 2012.